

# SCORE MATCHING VIA DIFFERENTIABLE PHYSICS

Benjamin Holzschuh<sup>1,2\*</sup> Simona Vegetti<sup>2</sup> Nils Thuerey<sup>1</sup>

<sup>1</sup>Technical University of Munich, Boltzmannstr. 3, 85748 Garching, Germany

<sup>2</sup>Max Planck Institute for Astrophysics, Karl-Schwarzschild-Strasse 1, 85748 Garching, Germany

## ABSTRACT

Diffusion models based on stochastic differential equations (SDEs) gradually perturb a data distribution  $p(\mathbf{x})$  over time by adding noise to it. A neural network is trained to approximate the score  $\nabla_{\mathbf{x}} \log p_t(\mathbf{x})$  at time  $t$ , which can be used to reverse the corruption process. In this paper, we focus on learning the score field that is associated with the time evolution according to a physics operator in the presence of natural non-deterministic physical processes like diffusion. A decisive difference to previous methods is that the SDE underlying our approach transforms the state of a physical system to another state at a later time. For that purpose, we replace the drift of the underlying SDE formulation with a differentiable simulator or a neural network approximation of the physics. We propose different training strategies based on the so-called probability flow ODE to fit a training set of simulation trajectories and discuss their relation to the score matching objective. For inference, we sample plausible trajectories that evolve towards a given end state using the reverse-time SDE and demonstrate the competitiveness of our approach for different challenging inverse problems.

## 1 INTRODUCTION

Many physical systems are time-reversible on a microscopic scale. For example, a continuous material can be represented by a collection of interacting particles (Gurtin, 1982; Blanc et al., 2002) based on which we can predict future states of the material. We can also compute earlier states, meaning we can evolve the simulation backwards in time (Martyna et al., 1996). When taking a macroscopic perspective, we only know the average quantities within specific regions (Farlow, 1993), which constitutes a loss of information. It is only then that time-reversibility is no longer possible, since many macroscopic and microscopic initial states exist that evolve to yield the same macroscopic state.

In the following, we target inverse problems to reconstruct the distribution of initial macroscopic states for a given end state. This genuinely tough problem has applications in many areas of scientific machine learning (Zhou et al., 1996; Gómez-Bombarelli et al., 2018; Delaquis et al., 2018; Lim & Psaltis, 2022), and existing methods lack tractable approaches to represent and sample the distribution of states. We address this issue by leveraging continuous approaches for diffusion models in the context of physical simulations. In particular, our work builds on the *reverse-diffusion* theorem (Anderson, 1982). Given the functions  $f(\cdot, t) : \mathbb{R}^d \rightarrow \mathbb{R}^d$ , called *drift*, and  $g(\cdot) : \mathbb{R} \rightarrow \mathbb{R}$ , called *diffusion*, it can be shown that under mild conditions, for the forward stochastic differential equation (SDE)  $d\mathbf{x} = f(\mathbf{x}, t)dt + g(t)dw$  there is a corresponding reverse-time SDE  $d\mathbf{x} = [f(\mathbf{x}, t) - g(t)^2 \nabla_{\mathbf{x}} \log p_t(\mathbf{x})]dt + g(t)d\tilde{w}$ . In particular, this means that given a marginal distribution of states  $p_0(\mathbf{x})$  at time  $t = 0$  and  $p_T(\mathbf{x})$  at  $t = T$  such that the forward SDE transforms  $p_0(\mathbf{x})$  to  $p_T(\mathbf{x})$ , then the reverse-time SDE runs backward in time and transforms  $p_T(\mathbf{x})$  into  $p_0(\mathbf{x})$ . The term  $\nabla_{\mathbf{x}} \log p_t(\mathbf{x})$  is called the *score*.

This theorem is a central building block for SDE-based diffusion models and denoising score matching (Song et al., 2021c; Jolicœur-Martineau et al., 2021), which parameterize the drift and diffusion in such a way that the forward SDE corrupts the data and transforms it into random noise. By training a neural network to represent the score, the reverse-time SDE can be deployed as a generative model, which transforms samples from random noise  $p_T(\mathbf{x})$  to the data distribution  $p_0(\mathbf{x})$ .

\*Correspondence to: benjamin.holzschuh@tum.de

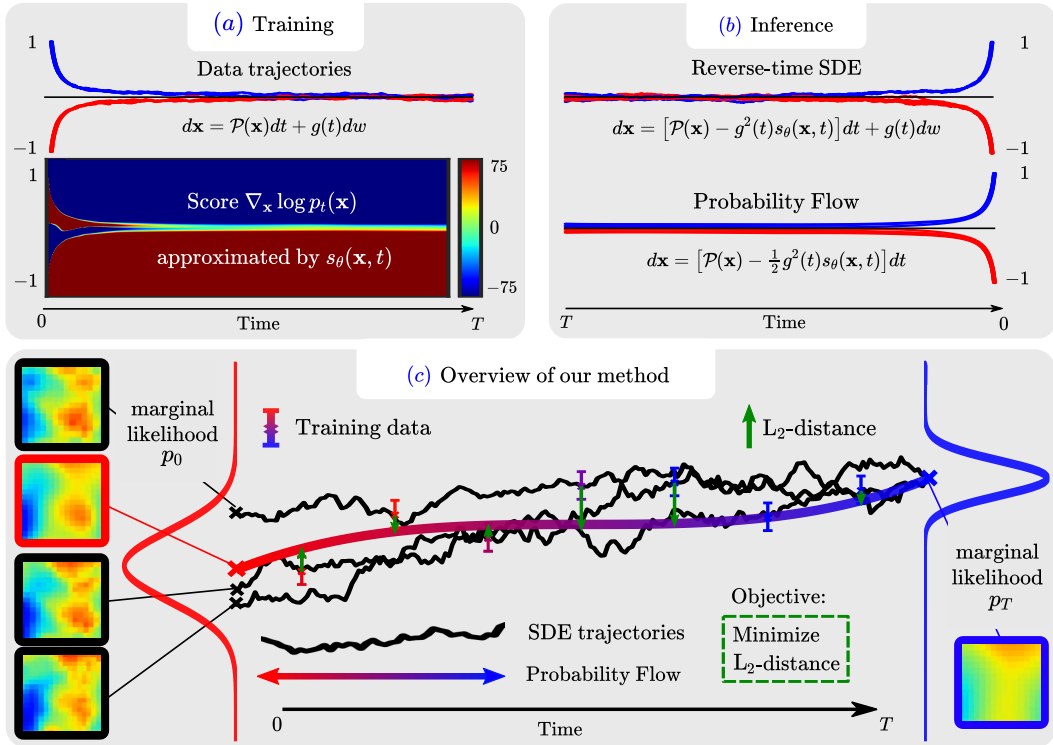


**Figure 1:** Overview. (a) Training with data set of trajectories and known temporal dynamics given by  $\mathcal{P}(\mathbf{x}) := -\text{sign}(\mathbf{x})\mathbf{x}^2$  and  $g \equiv 0.1$ . We estimate the score  $\nabla_{\mathbf{x}} \log p_t(\mathbf{x})$  with our proposed method using a neural network  $s_\theta(\mathbf{x}, t)$ . The colormap is truncated at  $-75$  and  $75$ . Negative values (blue) push down the trajectories and positive ones (red) push them up. Together with the dynamics, this can be used to reverse the system as shown in (b) either with the reverse-time SDE or the probability flow ODE. An overview how the training is performed is shown in (c). We minimize the  $L_2$ -distance between the probability flow ODE and samples from the SDE trajectories.

In this paper, we show that a similar methodology can likewise be employed to model physical processes. We replace the drift  $f(\mathbf{x}, t)$  by a time-independent physics model  $\mathcal{P}(\mathbf{x}) : \mathbb{R}^d \rightarrow \mathbb{R}^d$ , which is implemented by a differentiable solver or a neural network that represent the dynamics of the system, thus deeply integrating physical knowledge into our method. The end state at  $t = T$  on which the forward SDE acts is not fully destroyed by the diffusion  $g(t)$ , but instead, the noise acts as a perturbation of the system state over time.

Our method is very flexible by design and training can either be done using single simulation steps, similar to the training of traditional diffusion models, or be extended to rollouts for multiple steps, which requires the differentiability of the physics operator. We show that training with single steps directly relates to the score matching objective, while the extension to multiple steps corresponds to a maximum likelihood training of the probability flow ODE. We argue that considering multiple steps is important for the stability of the produced trajectories, as the implementation of the physics operator relies on temporal and spatial discretizations, which necessitates that physics and neural network interactions and feedback are included in the training. An overview of our method is shown in figure 1 for a simple toy problem (cf. appendix B).

To the best of our knowledge, our work is the first to leverage the reverse-diffusion theorem as a method for solving inverse problems of physical systems. We showcase the efficacy of the score matching viewpoint on physics problems with a range of challenging inverse problems. We refer to this perspective as *score matching via differentiable physics*, or *SMDP* in short. Specifically, our contributions are:

1. We leverage the reverse-diffusion theorem and score matching to solve inverse problems that involve the time evolution of physical systems. We demonstrate the competitiveness

of SMDP against common baseline approaches using the 2D heat equation with noise as an example.

2. Our approach gives new theoretical insights how learned corrector approaches for physical simulations can be interpreted in a probabilistic framework that connects the learned corrections to the score of the underlying data distribution.
3. We propose variants of SMDP, which can be used when the underlying physical system is deterministic, but still learn the score  $\nabla_{\mathbf{x}} \log p_t(\mathbf{x})$  of the data distribution.
4. We highlight the effectiveness of SMDP with a more challenging inverse problem where we simulate a fluid-based transport process backwards in time in the presence of randomized obstacles. Here, we compare our method to learned solvers.
5. Finally, we show that SMDP can even be used when the underlying physics are unknown. Our approach can be combined with operator learning methods and we demonstrate its effectiveness for learning the Navier-Stokes equation in the turbulent regime.

## 2 BACKGROUND AND RELATED WORK

**Learned solvers:** Numerical simulations benefit greatly from machine learning models (Tompson et al., 2017; Morton et al., 2018; Pfaff et al., 2020; Li et al., 2020). By integrating a neural network inside differential equation solvers, it is possible learn to reduce numerical errors (Tompson et al., 2017; Kochkov et al., 2021; Brandstetter et al., 2022) or guide the simulation towards a desired target state (Holl et al., 2020b; Li et al., 2022). As errors may accumulate quickly over time, trained networks benefit from gradients that are backpropagated over multiple time steps (Um et al., 2020).

**Diffusion models:** Diffusion models (Ho et al., 2020; Song et al., 2021c) have been considered for a wide range of applications. Most notably, diffusion models have been proposed for image (Dhariwal & Nichol, 2021), video (Ho et al., 2022; Höppe et al., 2022; Yang et al., 2022) and audio synthesis (Chen et al., 2021). Recently, Bansal et al. (2022) have proposed to train generalized diffusion models for arbitrary transformations and suggest that fully deterministic models without any noise are sufficient for generative behaviour. Specifically for uncertainty quantification, solving inverse problems and conditional sampling many methods have been proposed (Chung et al., 2021; 2022; Song et al., 2021b; Kwar et al., 2021; Ramzi et al., 2020). However, most approaches either focus on the denoising objective that is common for tasks involving natural images, or the synthesis process of solutions does not take the underlying physics directly into account.

**Reverse-time SDE and generative modeling via SDEs:** Classical denoising score matching approaches based on Langevin dynamics (Vincent, 2011; Song & Ermon, 2019, SMLD) and based on discrete Markov chains, e.g. Denoising Diffusion Probabilistic Models (Sohl-Dickstein et al., 2015; Ho et al., 2020, DDPM), can be unified in a time-continuous framework using SDEs (Song et al., 2021c). Given a distribution of states  $p_0(\mathbf{x})$  at time  $t = 0$ , an SDE transforms  $p_0(\mathbf{x})$  to a tractable distribution  $p_T(\mathbf{x})$

$$d\mathbf{x} = f(\mathbf{x}, t)dt + g(t)dw, \quad (1)$$

with  $w$  the standard Brownian motion, a drift  $f(\cdot, t) : \mathbb{R}^d \rightarrow \mathbb{R}^d$  and diffusion  $g(\cdot) : \mathbb{R} \rightarrow \mathbb{R}$ , which for  $\mathbf{x}_0 \sim p_0(\mathbf{x})$  yields a diffusion process  $(\mathbf{x}_t)_{t=0}^T$ . As outlined above, the reverse-time SDE of the reverse-diffusion theorem (Anderson, 1982) is given by

$$d\mathbf{x} = [f(\mathbf{x}, t) - g(t)^2 \nabla_{\mathbf{x}} \log p_t(\mathbf{x})]dt + g(t)d\tilde{w}, \quad (2)$$

with  $\nabla_{\mathbf{x}} \log p_t(\mathbf{x})$  being the *score*. By sampling from the tractable distribution  $p_T(\mathbf{x})$  and simulating the reverse-time SDE equation (2), we can generate samples from  $p_0(\mathbf{x})$ . Since the score  $\nabla_{\mathbf{x}} \log p_t(\mathbf{x})$  is not known analytically, it is approximated by a neural network  $s_\theta(\mathbf{x}, t)$  by minimizing the score matching objective

$$\mathcal{L}_{\text{SM}}(\theta) := \frac{1}{2} \int_0^T \mathbb{E}_{\mathbf{x} \sim p_t} [\|s_\theta(\mathbf{x}, t) - \nabla_{\mathbf{x}} \log p_t(\mathbf{x})\|_2^2] dt. \quad (3)$$

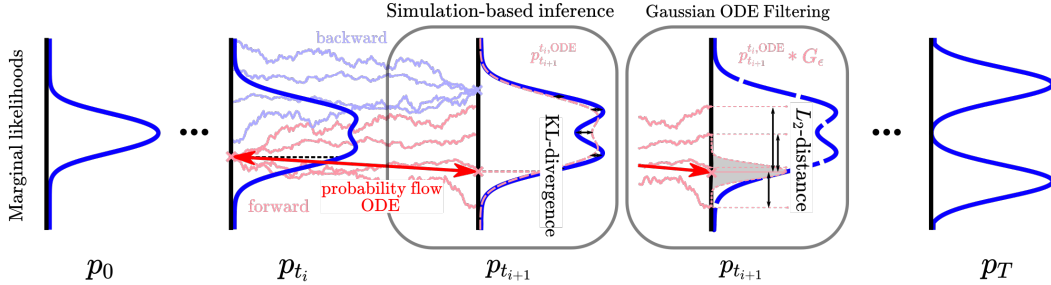


**Figure 2:** Illustration of single steps optimization. The optimization is split up into pairs of adjacent time steps. When considering  $p_{t_i}$  and  $p_{t_{i+1}}$  in the forward direction, our goal is to minimize the KL-divergence between  $p_{t_{i+1}}$  and the distribution  $p_{t_{i+1}}^{\text{ODE}}$  that is induced by simulating the probability flow ODE for samples drawn from  $p_{t_i}$ . Since ODEs are likelihood-free, simulation-based inference methods are required to optimize  $p_{t_{i+1}}^{\text{ODE}}$ . Note that a straightforward approach discards the relationship between  $p_{t_i}$  and  $p_{t_{i+1}}$ . Instead, we convolve  $p_{t_{i+1}}^{\text{ODE}}$  with the Gaussian kernel  $G_\epsilon$  and treat the conditional samples  $p_{t_{i+1}}^{\text{ODE}} | \mathbf{x}_{t_i}$  as a Gaussian distribution with mean  $\mu$ , which corresponds to the numerical solution of the probability flow ODE, and variance  $\sigma^2 := \epsilon > 0$ , i.e. Gaussian ODE filtering. This makes it possible to optimize the numerical solution of the ODE at  $t_{i+1}$  by estimating the  $L_2$ -distance of an ODE path to the SDE paths at  $t_{i+1}$  that start in the same point at  $t_i$ . For the single step optimization, we consider both the time forward and backward direction to learn the correct score. We extend this method with our multiple step formulation to allow for longer time horizons.

**Probability flow ODE and continuous normalizing flows:** Continuous normalizing flows (CNFs) are invertible generative models based on neural ODEs. Given an initial distribution  $z_0 \sim p_{z_0}(z_0)$  and a function  $f(z(t), t; \theta)$  represented by a neural network, a CNF is trained to solve the ODE  $\partial z(t)/\partial t = f(z(t), t; \theta)$  with boundary conditions  $z(t_0) = z_0$  and  $z(t_1) = \mathbf{x}$ , where  $\mathbf{x} \in \mathbb{R}^d$  is a sample from the training data set. A useful property of CNFs is that it is cheap to compute the log-likelihood of data samples, due to the instantaneous change of variables formula  $\partial \log p(z(t))/\partial t = -\text{Tr}(\partial f / \partial z(t))$  (Grathwohl et al., 2019).

The evolution of the marginal probability density  $p_t(\mathbf{x})$  for the SDE in equation (1) is described by Kolmogorov’s forward equation (Øksendal, 2003). Maoutsa et al. (2020) and Song et al. (2021c) show that there exists an ODE with the same Kolmogorov forward equation. This ODE is called *probability flow ODE* and is given by

$$d\mathbf{x} = \left[ f(\mathbf{x}, t) - \frac{1}{2} g(t)^2 \nabla_{\mathbf{x}} \log p_t(\mathbf{x}) \right] dt. \quad (4)$$

The probability flow ODE equation (4) represents a CNF and, if  $f(\mathbf{x}, t)$  is known, a network  $s_\theta$  parameterized by  $\theta$  representing  $\nabla_{\mathbf{x}} \log p_t(\mathbf{x})$  can be trained via maximum likelihood using standard methods (Chen et al., 2018). While the evolution of  $p_t(\mathbf{x})$  is the same between the probability flow ODE from equation (4) and the reverse-time SDE from equation (2), there are caveats due to the approximation by  $s_\theta(\mathbf{x}, t)$  (Song et al., 2021b; Lu et al., 2022). Huang et al. (2021) show that minimizing the score-matching loss is equivalent to maximizing a lower bound of the likelihood obtained by sampling from the reverse-time SDE. A recent variant combines score matching with CNFs (Zhang & Chen, 2021), and employs a joint training of the drift and score with an integration backwards in time.

### 3 METHOD

In this paper, we consider physical systems  $\mathbf{x}_t \in \mathbb{R}^d$  whose temporal evolution can be approximated using a physics operator  $\mathcal{P}(\mathbf{x}) : \mathbb{R}^d \rightarrow \mathbb{R}^d$ , i.e.  $\mathbf{x}_{t+\Delta t} \approx \mathbf{x}_t + \Delta t \mathcal{P}(\mathbf{x}_t)$ . The physics operator can be implemented as a PDE solver for analytically known underlying dynamics or learned directly from the data using e.g. operator learning approaches. We assume that  $\mathcal{P}$  is differentiable. While we show that our method can be applied if  $\mathcal{P}$  is not differentiable, we argue that including physics and neural network interactions in the training, which requires differentiability, improves the overall performance. The system states are perturbed using a small additive Gaussian noise, which allows

us to embed the time evolution of the physical system in a stochastic differential equation

$$d\mathbf{x} = \mathcal{P}(\mathbf{x})dt + g(t)dw, \quad (5)$$

with a diffusion process  $g(\cdot) : \mathbb{R} \rightarrow \mathbb{R}$ . The diffusion can be regarded as either noise inherent to the physics (e.g. when modeling chaotic systems), or as noise coming from a measurement process. In our method, it is also possible to set  $g(t) = 0$  for a range of values  $t$  which makes the evolution deterministic. We can simulate paths from this SDE similar to ODEs using Euler-Maruyama steps, i.e. for initial state  $\mathbf{x}_0$  and time discretization  $t_0 < t_1 < \dots < t_M$  with  $t_0 = 0$  and  $t_M = T$ , we obtain the iteration rule

$$\mathbf{x}_{t_{m+1}} \leftarrow \mathbf{x}_{t_m} + (t_{m+1} - t_m) \mathcal{P}(\mathbf{x}_{t_m}) + \sqrt{t_{m+1} - t_m} g(t_m) z_{t_m}, \quad (6)$$

where  $z_{t_m}$  are i.i.d. with  $z_{t_m} \sim \mathcal{N}(0, I)$ .

As training data, we consider a set of  $N$  trajectories  $\{\{\mathbf{x}_{t_i, n}\}_{i=0, \dots, M}\}_{n=0, \dots, N}$  sampled with equation (6), which describe our system states at a fixed time discretization.

**Inverse Problem** Given an end state  $\mathbf{x}_T$  of the system, we are interested in recovering a likely trajectory  $(\mathbf{x}_{t_i}^{\text{pred}})_{i=0, \dots, M}$  that evolves towards  $\mathbf{x}_T$ . More formally, the set of trajectories  $\{\{\mathbf{x}_{t_i, n}\}_{i=0, \dots, M}\}_{n=0, \dots, N}$  implicitly defines marginal likelihoods  $p_t(\mathbf{x})$  at every time step  $t$  which are linked through the SDE equation (5) of the physical system by the Kolmogorov forward equation (Øksendal, 2003). The solution trajectory may not be unique, so we want to sample from the full posterior instead of obtaining only a maximum likelihood solution, i.e. we want to sample from  $p_0(\mathbf{x} | \mathbf{x}_T)$ . To do so, we learn a function  $s_\theta(\mathbf{x}, t)$  represented by a neural network that approximates the score  $\nabla_{\mathbf{x}} \log p_t(\mathbf{x})$ . Then, we can simulate paths starting in  $\mathbf{x}_T$  from the reverse-time SDE introduced in section 2 with  $s_\theta(\mathbf{x}, t)$  plugged in for the score

$$d\mathbf{x} = [\mathcal{P}(\mathbf{x}) - g^2(t)s_\theta(\mathbf{x}, t)] dt + g(t)dw. \quad (7)$$

It follows from the reverse-diffusion theorem (Anderson, 1982) that equation (7) yields the correct posterior distribution for our inverse problem.

**Single steps** Unlike SDE-based diffusion models where the score is available analytically, we consider arbitrary physics operators. We leverage the fact that the evolution of the marginal likelihoods  $p_t$  of the reverse-time SDE and the probability flow ODE are the same, see e.g. (Song et al., 2021c). Additionally, the probability flow ODE is deterministic and defines a bijective mapping. We replace the score inside the probability flow ODE equation (4) by a neural network approximation  $s_\theta(\mathbf{x}, t)$  and define  $p_{t_i}^{t_j, \text{ODE}}$  as the distribution obtained by sampling from  $p_{t_j}$  and solving the ODE until  $t_i$ . In this definition, we allow that  $i > j$  in which case we integrate the ODE backwards in time.

For single steps, we want that  $p_{t_{i+1}}$  is close to  $p_{t_{i+1}}^{t_i, \text{ODE}}$  as well as that  $p_{t_{i-1}}$  is close to  $p_{t_{i-1}}^{t_i, \text{ODE}}$ , i.e. that the probability flow ODE correctly matches the right distribution no matter if we solve it forward or backward in time. To optimize this case, we consider the objective of minimizing the Kullback-Leibler divergence between the joint distributions, which we denote using the symbol  $\times$ , i.e.

$$\text{KL}(p_{t_{i-1}} \times p_{t_i} \| p_{t_{i-1}}^{t_i, \text{ODE}} \times p_{t_i}) + \text{KL}(p_{t_i} \times p_{t_{i+1}} \| p_{t_i} \times p_{t_{i+1}}^{t_i, \text{ODE}}). \quad (8)$$

The instantaneous change of variables formula that transforms the densities is of no help here, as no marginal likelihoods  $p_t$  can be computed analytically for this scenario. Since ODEs are deterministic and therefore likelihood-free, simulation-based inference methods, which are slow and costly, are often necessary for optimization. In this paper, we use Gaussian ODE filtering, which slightly perturbs the ODEs (Kersting et al., 2020), to efficiently compute gradients for optimization. The conditional probabilities  $p_{t_i}^{t_j, \text{ODE}}(\mathbf{x} | \mathbf{x}_{t_j})$  can then be modeled as Gaussians with mean  $\mu^{\text{ODE}}(\mathbf{x}_{t_j})$  the numerical solution of the probability flow ODE for a given ODE solver and variance  $\sigma^2 := \epsilon > 0$ . A possible interpretation of the perturbation  $\epsilon$  is that it corresponds to a Laplace approximation of the errors introduced by numerical inaccuracies (Conrad et al., 2017). As  $\epsilon \rightarrow 0$  the conditional distribution converges to a Dirac Delta distribution centered on the correct solution. Given slices  $(\mathbf{x}_{t_{i-1}}, \mathbf{x}_{t_i}, \mathbf{x}_{t_{i+1}})$  sampled from the training trajectories, our loss for training is

$$\mathcal{L}_{\text{single}}(\theta) = \mathbb{E}_{(\mathbf{x}_{t_{i-1}}, \mathbf{x}_{t_i}, \mathbf{x}_{t_{i+1}})} \left[ \|\mathbf{x}_{t_{i+1}} - \mu_{t_{i+1}}^{\text{ODE}, \text{F}}(\mathbf{x}_{t_i})\|_2^2 + \|\mathbf{x}_{t_{i-1}} - \mu_{t_{i-1}}^{\text{ODE}, \text{B}}(\mathbf{x}_{t_i})\|_2^2 \right], \quad (9)$$

where  $\mu_{t_{i+1}}^{\text{ODE,F}}$  is integrated forward in time and  $\mu_{t_{i-1}}^{\text{ODE,B}}$  backwards in time. Importantly, the loss we derive from this formulation is independent of  $\epsilon$ . In appendix A.2, we show that this is an unbiased estimator for equation (8) up to a constant factor depending on  $\epsilon$  and optimizing it is equivalent to minimizing the score matching objective equation (3) if  $\Delta t$  is small.

**Multiple steps** In regular diffusion models and the single step formulation of our method, there are no feedback loops between the neural network  $s_\theta(\mathbf{x}, t)$  and the drift. Since, in our case, the drift is represented by an arbitrary physics operator, which may have a bad conditioning, numerical errors can accumulate over time, and the trajectories diverge from the training domain during inference. For this reason, feedback loops between the physics solver, implemented e.g. with a differentiable PDE solver, and the neural network should be considered (Um et al., 2020). Our single step loss formulation can be extended to multiple steps in the following way: for a sequence  $(\mathbf{x}_{t_i}, \mathbf{x}_{t_{i+1}}, \dots, \mathbf{x}_{t_j})$  and  $i < j$ , we consider the loss

$$\mathcal{L}_{\text{multi}}(\theta) = \mathbb{E}_{(\mathbf{x}_{t_i}, \dots, \mathbf{x}_{t_j})} \left[ \sum_{k=i+1}^{j-1} \|\mathbf{x}_{t_k} - \mathbf{x}_{t_k}^{\text{ODE,F}}(\mathbf{x}_{t_i})\|_2^2 + \|\mathbf{x}_{t_k} - \mathbf{x}_{t_k}^{\text{ODE,B}}(\mathbf{x}_{t_j})\|_2^2 \right] \quad (10)$$

$$\text{s.t. } \mathbf{x}_{t_j}^{\text{ODE,F}} = \mathbf{x}_{t_i} + \int_{t_i}^{t_j} \mathcal{P}(\mathbf{x}_t^{\text{ODE,F}}) - \frac{1}{2}g^2(t)s_\theta(\mathbf{x}_t^{\text{ODE,F}}, t)dt, \quad (11)$$

$$\text{and } \mathbf{x}_{t_i}^{\text{ODE,B}} = \mathbf{x}_{t_j} + \int_{t_j}^{t_i} \mathcal{P}(\mathbf{x}_t^{\text{ODE,B}}) - \frac{1}{2}g^2(t)s_\theta(\mathbf{x}_t^{\text{ODE,B}}, t)dt, \quad (12)$$

This objective is similar to the loss used for learned corrector approaches, but includes optimizing both increasing and decreasing time directions. We show in appendix A.3 that while this loss does not directly optimize the score matching objective, under the same assumptions as the single step updates, it improves a variational lower bound on the maximum likelihood training of the corresponding continuous normalizing flow. If  $s_\theta(\mathbf{x}_t, t) \equiv \nabla_{\mathbf{x}} \log p_t(\mathbf{x}_t)$ , it follows from the general theory of probability flow ODEs (Song et al., 2021a) that all marginal likelihoods coincide with the SDE and  $s_\theta(\mathbf{x}_t, t)$  is a maximizer for the maximum likelihood training.

**Sliding window training** The single step and multiple step formulation do not directly rely on the simulation start and end time. Importantly, we can think of the probability flow ODE from time 0 to  $T$  as multiple, shorter ODEs that are chained together, e.g. from time 0 to  $t_1$ ,  $t_1$  to  $t_2$  etc. Correspondingly, our training uses a sliding window of size  $S$  that covers up to  $S$  elements of the training trajectories for batch of training samples and the multi step formulation. After updating  $\theta$  based on the loss, the window is moved by one. Once the entire trajectories has been covered, we continue with the next batch. In practice, we start training with a sliding window of size 2, which resembles the single step formulation. Then, after convergence, if we observe that during inference trajectories diverge from the correct solution domain, we gradually increase the sliding window size to account for longer feedback loops of the physics and neural network.

**SDE training** Training with the single step and multi step losses based on the probability flow ODE involves integrating the ODE forwards and backwards in time. Alternatively, we can directly optimize the reverse-time SDE. In this case, we drop the terms in the single step and multi step loss that correspond to the forward time direction and modify the constraints on the trajectory in the single step loss and multi step loss, i.e. equation (12), such that the trajectory is sampled from the reverse-time SDE instead of it solving the probability flow ODE. We give more details on this in appendix A.5.

**Inference** Given an end state  $\mathbf{x}_T$ , we can solve the probability flow ODE backwards in time using the trained score function  $s_\theta(\mathbf{x}, t)$  to obtain a trajectory  $(\mathbf{x}_{t_i}^{\text{pred}})_{i=0, \dots, M}$ . However, this will only give a single, deterministic solution and not allow for sampling from the posterior  $p(\mathbf{x} | \mathbf{x}_T)$ . Instead, we simulate trajectories from the reverse-time SDE equation (7). The evolution of marginal probabilities  $p_i(\mathbf{x})$  for this SDE is the same as for the probability flow ODE equation (4) (Song et al., 2021c). Moreover, by the reverse-diffusion theorem (Anderson, 1982), SDE equation (7) is the time-reverse of the physical system SDE from equation (5). Therefore, we can approximate sampling from  $p(\mathbf{x} | \mathbf{x}_T)$  by simulating trajectories from SDE equation (7) using any traditional SDE solver. In the following, we refer to the integration of the physics model  $\mathcal{P}(\mathbf{x})$  into the score-based

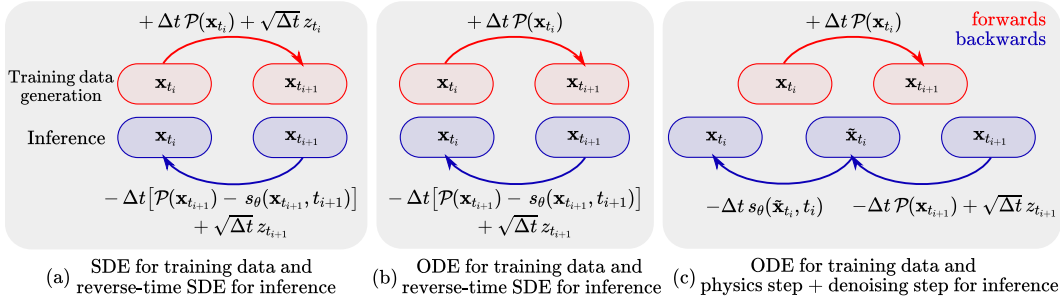


**Figure 3:** Variants of SMDP for different physical systems. (a) shows the SDE and reverse-time SDE setup with the Euler-Maruyama discretization when the system is modeled by an SDE. The diffusion term  $g(t)$  is absorbed in the Gaussian random variable  $z_t \sim \mathcal{N}(0, g(t)^2 T)$  and network  $s_\theta(\mathbf{x}, t)$ . In (b), we assume that the temporal evolution of the training data is deterministic, i.e. we model the physical system without the diffusion term. However, for inference we consider the reverse-time SDE of the same form as in (a), where the diffusion coefficient  $g(t)$  is chosen as a hyperparameter that depends on the measurement noise. Then, in (c), we split the Euler step for the backwards direction into a physics only update, adding the Gaussian noise  $z$ , and a denoising step by  $s_\theta(\mathbf{x}, t)$ .

modelling approach as *score matching via differentiable physics*, or *SMDP* in short. We denote trajectories from the probability flow ODE by *SMDP-ODE*, and those obtained by simulating the reverse-time SDE by *SMDP-SDE*.

**Variants for deterministic physical systems** So far, we have considered to model the physical system as an SDE, cf. equation (5), which allowed us to apply the reverse-diffusion theorem and use the reverse-time SDE for inference, see figure 3a. While this problem setup is suitable for many scenarios, we would also like to apply a similar methodology when the system is deterministic. In case of chaotic dynamical systems, this still represents a hard inverse problem, especially when there is a loss of information due to measurement noise. In figure 3b and figure 3c, we illustrate two additional variants of SMDP with deterministic physical systems. Figure 3b considers deterministic training trajectories from the forward evolution of the simulation. The only change required to transfer the single and multi step losses to this variant is to omit all terms that depend on the forward time direction. Since the forward evolution is now deterministic. While this means that the reverse-diffusion theorem can no longer be applied and we lose the theoretical result that the correct posterior can be obtained from the reverse-time SDE, this variant is interesting to provide empirical results. We lastly consider a full variant that separates the update by  $\mathcal{P}(\mathbf{x})$  and  $s_\theta(\mathbf{x}, t)$  into multiple steps in figure 3c. The temporal evolution from  $t_{i+1}$  to  $t_i$  is then defined entirely by the physics. We apply an additive noise to the system and the update step by  $s_\theta(\mathbf{x}, t)$ , which can be interpreted as denoising for a now slightly perturbed state  $\tilde{\mathbf{x}}_{t_i}$ . In this case, we show that the network  $s_\theta(\mathbf{x}, t)$  still learns the correct score  $\nabla_{\mathbf{x}} \log p_t(\mathbf{x})$  during training, see appendix A.6 for details. For inference, this method alternates between applying physics, adding noise, and the denoising step.

## 4 EXPERIMENTS

We conduct several experiments to demonstrate the advantages of SMDP compared to a number of baseline methods. We first consider the 2D heat equation in section 4.1 modeled by an SDE, where our objective is to find possible initial states at time  $t = 0$  given a noisy end state at time  $t = T$ . We additionally perform an ablation study for the sliding window size for the multi step loss  $\mathcal{L}_{\text{multi}}(\theta)$  as well as an ablation study for different modifications of the training and inference.

In our second experiment in section 4.2, we analyse a more challenging problem, where we are interested in reconstructing the trajectory of a deterministic buoyancy-driven flow within a closed simulation domain given an end state at time  $T$ . What makes this problem challenging is that for each simulation, we place different obstacles at different positions within the simulation domain. We evaluate different variants of SMDP based on the deterministic training set and compare against learned solvers.

Then, in section 4.3, we consider the situation where the physics of the system is unknown. For this purpose, we train a network that approximates the solutions to the Navier-Stokes equations using operator learning and a network that approximates the score field. We demonstrate that by doing so, we obtain an improved performance for inverse problems and the learned score can be used to refine predictions in post-processing.

#### 4.1 HEAT EQUATION

We consider the heat equation  $\frac{\partial u}{\partial t} = \alpha \Delta u$  which plays a fundamental role in many physical systems. Here, we set the diffusivity constant to  $\alpha = 1$  and initial conditions at  $t = 0$  are generated from Gaussian random fields with  $n = 4$  at resolution  $32 \times 32$ . We simulate the heat diffusion with noise, modeled as an SDE, using a spectral method until  $t = 0.2$  with a fixed step size  $\Delta t = 6.25 \times 10^{-3}$  using the iteration rule from equation (6) with  $g \equiv 0.1$ . The small noise contributions at each step are smoothed by the dynamics of the heat diffusion and have only a negligible effect on the simulation end state. Our training data set consists of 2,500 initial conditions with their corresponding trajectories and end states at  $t = 0.2$ . The test set is comprised of 500 initial conditions and corresponding end states generated directly without any noise, i.e.  $g \equiv 0$ .

The physics operator  $\mathcal{P}(\mathbf{x})$  is approximated using a spectral solver  $\mathcal{S}(\mathbf{x}, \Delta t)$  (details in appendix E). The spectral solver computes the correct solution that moves the simulation state  $\mathbf{x}$  forward in time by  $\Delta t$  based on the power spectrum of  $\mathbf{x}$ . However, we cannot use the spectral solver  $\mathcal{S}(\mathbf{x}, \Delta t)$  directly to infer the initial simulation state given the end state, since high frequencies due to noise will be amplified, leading to physically implausible solutions. We approximate the physics operator by

$$\mathcal{P}(\mathbf{x}) \approx (\mathcal{S}(\mathbf{x}, \Delta t) - \mathbf{x}) / \Delta t. \quad (13)$$

This approximation has the advantage that when using Euler steps for the ODE and SDE solver with step size  $\Delta t$ , the solutions are very accurate and this approach can be applied for a wide variety of physical systems and solvers. On the other hand, during training of  $s_\theta(\mathbf{x}, t)$ , the correct score depends on  $\mathcal{P}(\mathbf{x})$ , which depends on  $\Delta t$ . Thus,  $s_\theta(\mathbf{x}, t)$  can overfit on the step size  $\Delta t$ .

**Training** We consider a small *ResNet*-like architecture based on an encoder and decoder part (see appendix D) as representation for the score function  $s_\theta(\mathbf{x}, t)$ . The spectral solver is implemented via differentiable programming in *JAX* (Schoenholz & Cubuk, 2020). For better comparison with the baseline methods, these are trained with a Gaussian random noise with standard deviation  $\sigma = 0.1$  added to the inputs. This noise is applied to all simulation ends states, including SMDP, during testing.

**Baseline methods** As baseline methods, we consider the ResNet-like architecture from above, in addition to a *Bayesian neural network* (BNN) based on a U-Net architecture with spatial dropout (Mueller et al., 2022), as well as a *Fourier neural operator* (FNO) network (Li et al., 2020). For each of these three methods, we consider two variants: the first variant is trained with a *supervised loss*, i.e. the training data consists of pairs  $(\mathbf{x}_0, \mathbf{x}_T)$  with initial state  $\mathbf{x}_0$  and end state  $\mathbf{x}_T$ . The supervised loss corresponds to the squared L2 distance between the network prediction  $\mathbf{x}_0^{\text{pred}}$  and the ground truth, i.e.  $(\mathbf{x}_0^{\text{pred}} - \mathbf{x}_0)^2$ . For the second variant, the *reconstruction loss*, we rely on the differentiable solver and only make use of the end state  $\mathbf{x}_T$  such that the loss becomes  $(\mathcal{P}(\mathbf{x}_0^{\text{pred}}; T) - \mathbf{x}_T)^2$ , i.e we

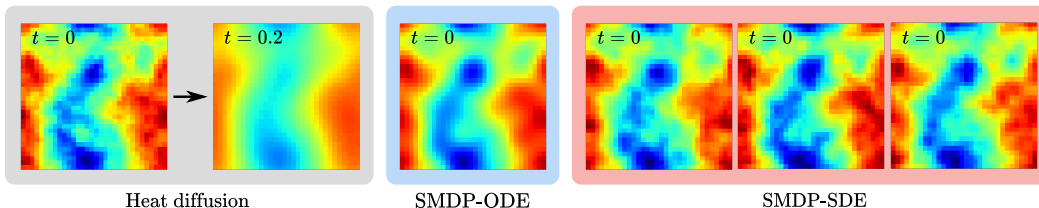


**Figure 4:** Heat diffusion case. We simulate a Gaussian random field at  $t = 0$  forwards in time using equation (6). Given  $s_\theta(\mathbf{x}, t)$ , we can either solve the probability flow ODE or simulate trajectories of the reverse-time SDE to obtain solutions for the state at  $t = 0$ .



Method	MSE [ $10^{-5}$ ] ↓	Spectral error ↓	Full posterior
SMDP-ODE	<b>0.79</b>	2.10	✗
SMDP-SDE	5.56	<b>0.21</b>	✓
ResNet-S	2.17	1.23	✗
ResNet-P	2.30	0.79	✗
BNN-S	347.00	1.16	✓
BNN-P	381.00	1.07	✓
FNO-S	25 400.00	1.60	✗
FNO-P	25 000.00	1.47	✗
HeatGen	1.39	2.87	✗
HeatGen+noise	4.45	1.89	✓

**Table 1:** Evaluation of reconstruction MSE and spectral error for SMDP and baselines. The column full posterior indicates whether models yield point estimates or allow to sample from the posterior.

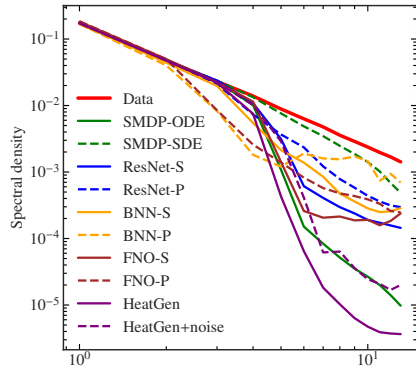


**Figure 5:** Spectral density on different scales, the red line indicating ground truth. The closer a method is to the ground truth, the better it produces structures of a similar scale.

simulate the network output forward in time using  $\mathcal{P}$  to obtain a state at  $t = T$ , which we compare to the desired end state  $\mathbf{x}_T$ . We denote the supervised variant by  $S$  and the physics-based one by  $P$ . Additionally, we consider a generative model, similar to Rissanen et al. (2022), denoted by *HeatGen*. We train this network analogously to SMDP-ODE, but without the physics  $\mathcal{P}$ , such that the network learns the score and the physics at the same time.

**Reconstruction accuracy vs. fitting the data manifold** We give an evaluation of our method and the baselines by considering the *reconstruction MSE* on the test set: how well a predicted initial state  $\hat{\mathbf{x}}_0$  that is simulated forward in time yields states that correspond to the reference end state  $\mathbf{x}_T$  in terms of MSE. This metric has the disadvantage that it does not measure how well the prediction matches the training data manifold, i.e. for this case whether the prediction resembles the statistics of the Gaussian random field. For that reason, we additionally compare the power spectral density of the states as the *spectral loss*. The corresponding measurements are given in table 1, which show that our method SMDP-ODE performs best in terms of the reconstruction MSE. However, solutions obtained by SMDP-ODE are very smooth and do not contain the small-scale structures of the references, which is reflected in a high spectral error that is also visually prominent, as shown in figure 5. SMDP-SDE on the other hand performs very well in terms of spectral error and yields visually convincing solutions with only a slight increase in the reconstruction loss. We note that there is a natural tradeoff between both metrics, and SMDP-ODE and SMDP-SDE perform best for both cases respectively while using the same set of weights. We include additional experiments with the 1D heat equation in appendix C, where we qualitatively analyze the full posterior distribution obtained from SMDP-SDE.

**Ablation: Inference and Training** The single and multi step formulations of the training of  $s_\theta(\mathbf{x}, t)$  require solving the probability flow ODE forward and backward in time (cf. equations 9 and 10). We consider two additional variants of the training. As the first variant, we train SMDP based on the probability flow, but only for the backward direction, i.e. dropping the term  $\|\mathbf{x}_{t_i} - \mu_{t_i}^{\text{ODE},F}(\mathbf{x}_{t_{i-1}})\|_2^2$  in equation (9) and equation (10) respectively. We show in appendix A.5 that in this case the network  $s_\theta(\mathbf{x}, t)$  learns  $2\nabla_{\mathbf{x}} \log p_t(\mathbf{x})$  instead of  $\nabla_{\mathbf{x}} \log p_t(\mathbf{x})$  and we correct for this during inference. Moreover, we consider the SDE training, which directly optimizes the reverse-time SDE. For the single step formulation, by our theory, all three variants learn the correct score, but might differ for the multi step formulation. An evaluation in terms of reconstruction MSE and spectral loss is shown in figure 6.

We evaluate four methods for inference, which include SMDP-ODE and SMDP-SDE. Additionally, we consider the reverse-time SDE, but during inference set all drawn noise terms in the Euler-Maruyama discretization to 0 (labeled *Reverse-time ODE*). Finally, we consider the probability flow ODE, but add a noise term analogous to the SDE for each Euler step (labeled *Probability flow SDE*). In practice, all methods only differ by their weighting for the score  $s_\theta(\mathbf{x}, t)$  and noise standard

deviation for inference. We vary  $\Delta t$ , i.e. the number of steps (1x corresponds to 32 inference steps, 2x to 64 and so on).

Overall, our evaluations shows that there are only small differences between the backward only probability flow and SDE training, cf. figure 6b and 6c. The probability flow inference (SMDP-ODE) fares badly in both cases. We believe that this is due to an overfitting of the network to the time discretization used to approximate  $\mathcal{P}(\mathbf{x})$ , see equation (13), which causes problems when having a different weighting of the score during inference than during training. For the probability flow training of the network figure 6a, the results for both the ODE and SDE inference are more stable. In particular, since the networks are trained with a network weighting of  $1/2$ , i.e. according to the probability flow formulation, when the weighting is increased for the reverse-time SDE during inference, all contributions learned by  $s_\theta(\mathbf{x}, t)$  due to an overfitting on the time discretization are overestimated. Therefore, the SDE inference methods are less accurate in this case than for the SDE training. On the other hand, if the contributions due to time discretizations are overestimated, the inference seems to produce more stable trajectories and is more robust when the time discretization is changed, e.g.  $\Delta t$  is divided by a power of 2. This effect is not seen for the backwards only probability flow and SDE training.

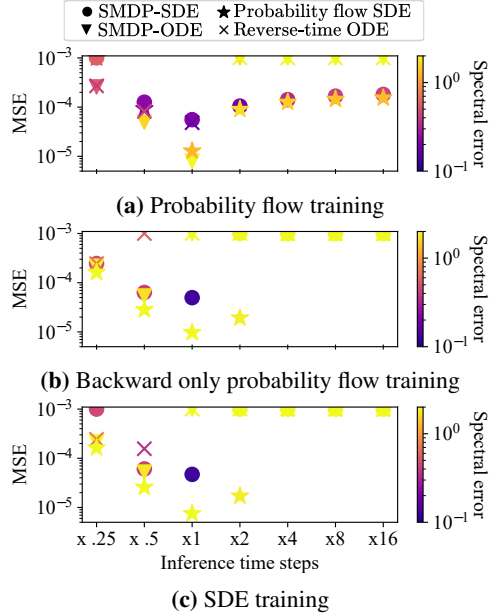


**Figure 6:** Heat equation reconstruction MSE and spectral error averaged over 3 runs for different training and inference methods. Training was done with 32 steps for a single simulation.

**Ablation: Sliding Window** We performed an ablation study on the sliding window method and the window size  $S$ , also called rollout length. Additionally, we evaluate the effect of cutting gradients early, i.e. it is possible to unroll the sliding window for  $S$  steps, but stop the gradient backpropagation after  $G < S$  steps. E.g., for  $S = 32$  steps, we can compute the first  $G = 8$  steps, save the intermediate results, then backpropagate the gradient to optimize  $\theta$ . Then, we continue with the intermediate results as a new initialization, again stopping and updating  $\theta$  after  $G$  steps. In this example, we can repeat this  $S/G = 4$  times in total until we obtain the entire window of  $S$  steps. An advantage of stopping the gradient after  $G$  steps is that it reduces memory requirements, as we do not need to store all intermediate results and therefore this allows for training with large window sizes. In figure 7, we show the results on the reconstruction MSE for SMDP-ODE and SMDP-SDE. We keep the time discretization fixed, i.e. a full simulation trajectory consists of 32 steps from  $t = 0$  until  $t = 0.2$ , however we vary the window size  $S$ . In this case, we always backpropagate gradients through all unrolling steps. In the second case, where we change the number of gradient backpropagation steps, we keep the window size  $S$  fixed at 32, which is the entire simulation trajectory. For both SMDP-ODE and SMDP-SDE, our evaluation shows that both longer rollouts and more gradient backpropagation steps improve the reconstruction MSE. The improvements are more significant for SMDP-SDE.

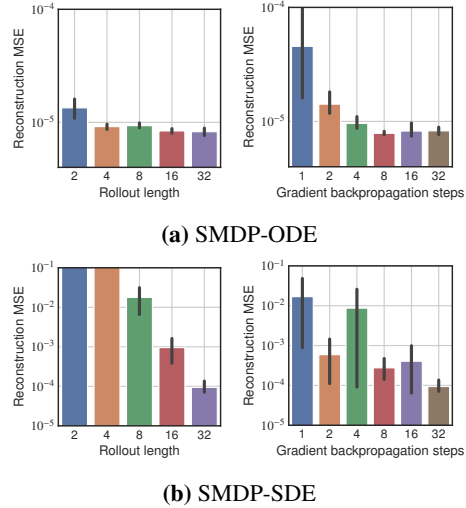


**Figure 7:** Heat equation reconstruction MSE averaged over 5 runs for different sliding window sizes  $S$  (rollout length) and number of gradient backpropagation steps for SMDP-ODE (a) and SMDP-SDE (b).

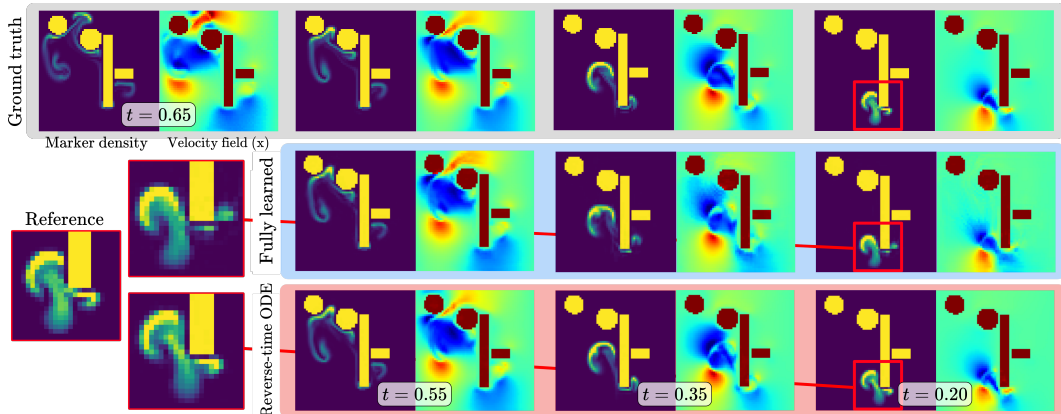


**Figure 8:** Buoyancy flow case. Ground truth shows the marker density and velocity field in the  $x$ -direction at different points of the simulation trajectory from the test set. The simulation end state at  $t = 0.65$  is the input for inference via the learned solver (fully learned) and SMDP (reverse-time ODE).

## 4.2 BUOYANCY-DRIVEN FLOW WITH OBSTACLES

Next, we test our methodology on a more challenging problem. For this purpose we consider deterministic simulations of buoyancy-driven flow within a fixed domain  $\Omega \subset [0, 1] \times [0, 1]$  and randomly placed obstacles. We make use of semi-Lagrangian advection for the velocity and MacCormack advection for the hot marker density. The temperature dynamics of the marker field are modeled with a Boussinesq approximation. Each simulation runs from time  $t = 0.0$  to  $t = 0.65$  with a step size of  $\Delta t = 0.01$ . The inflow at  $(0.2, 0.5)$  is active until  $t = 0.2$ . Our objective is to employ SMDP to obtain trajectories that reconstruct a plausible flow given an end state of the marker density and velocity fields at time  $t = 0.65$ .

**Training** Our training data set consists of 250 simulations with corresponding trajectories. Since trajectories are generated from a deterministic simulation, we add a Gaussian measurement noise to each simulation state  $\mathbf{x}_t$  with  $\sigma_t = \sqrt{\Delta t}$ . To run the simulation, we make use of the differentiable *phiflow* solver (Holl et al., 2020a). We place spheres and boxes with varying sizes at different positions within the simulation domain that do not overlap with the marker inflow. For each simulation, we place one to two objects of each category. The test set comprises 5 simulations. We consider the three different training variants from figure 3. The network  $s_\theta(\mathbf{x}, t)$  is trained based on the probability flow without any modifications, then when only considering the backward direction for the probability flow and third, based on splitting the physics and score steps in the Euler step discretization as shown in figure 3c.

Our neural network architecture for  $s_\theta(\mathbf{x}, t)$  uses dilated convolutions (Stachenfeld et al., 2021), see appendix D for details. The physics operator step  $-\Delta t \mathcal{P}(\mathbf{x})$  is implemented directly in the solver by using a negative step size  $-\Delta t$  for time integration. For the sliding window size, we start with  $S = 2$  and increase  $S$  by 2 every 30 epochs until we reach 20. See appendix F for additional training details. We compare our method to learned solvers, labeled *Fully learned*, for which we train  $s_\theta(\mathbf{x}, t)$  with the multi step loss and sliding window method, but do not include the physics operator  $\mathcal{P}(\mathbf{x})$ , which has to be learned by  $s_\theta(\mathbf{x}, t)$ . Additionally, we directly invert the physics of the system, labeled *Physics only*, which only utilizes  $\mathcal{P}(\mathbf{x})$  and no learned components.

**Evaluation** A quantitative evaluation in terms of reconstruction MSE and LPIPS metrics (Zhang et al., 2018) is given in figure 9. For the reconstruction MSE, we simulate the predicted initial state forward in time again and calculate the  $L_2$ -distance to the given end state.

The *physics only* variant is not capable of yielding good predictions, even when ignoring effects due to noise. This shows in a high reconstruction MSE and LPIPS distance. With our training setup, the *fully learned* variant compares very well and is also able to obtain good results, which are even slightly better than for the the probability flow based training. There are several reasons, why including the physics  $\mathcal{P}$  in the probability flow training does not pay off in this case. First,

during training we optimize both time directions, which makes sense if the underlying physical system is modeled as an SDE. However for this task, optimizing the forward direction deteriorates the performance. Second, for the probability flow training, we require that  $\Delta t$  is sufficiently small and the physics backward step is stable and accurate. Both these conditions are not fully satisfied here.

This also explains, why the reverse-time SDE and ODE solutions for which the weighting of  $s_\theta(\mathbf{x}, t)$  is modified, perform poorly. The network  $s_\theta(\mathbf{x}, t)$  overfits on  $\Delta t$  and additionally learns substantial corrections to the comparatively inaccurate reverse physics step. We note, that even though in terms of reconstruction MSE and LPIPS, the reverse-time SDE and ODE solutions compare badly, visually they are still convincing and a major improvement to the *physics only* version, cf. figure 21 in the appendix.

The models based on the backwards only probability flow training and splitting the physics and score update perform very well with clear advantages over the *fully learned* version. The reverse-time ODE inference solutions have significantly lower reconstruction MSEs and LPIPS distances, while for the reverse-time SDE inference, the solutions are on par with the *fully learned* method, even though applying the noise during inference makes the task significantly harder. The higher LPIPS distances can be explained by the included noise, which is still noticeable in the solutions and greatly increases the distance, but could be filtered out easily via post-processing.

### 4.3 ISOTROPIC TURBULENCE

As third example, we consider a problem where the physics operator is unknown, i.e. we approximate both  $\mathcal{P}(\mathbf{x})$  and the score  $\nabla_{\mathbf{x}} \log p_t(\mathbf{x})$  by neural networks. We consider the problem of learning the time evolution of isotropic, forced turbulence as determined by the 2D Navier-Stokes equations with a viscosity of  $\nu = 10^{-5}$  (Li et al., 2020). The training data set consists of vorticity fields from 1000 simulation trajectories from  $t = 0$  until  $T = 10$  with  $\Delta t = 1$  and a spatial resolution of  $64 \times 64$ . Our objective is to predict a trajectory  $\hat{\mathbf{x}}_{0:10}$  that reconstructs the true trajectory  $\mathbf{x}_{0:10}$  given an end state  $\mathbf{x}_{10}$  of the solution, whereas in the original paper, the objective was to learn an operator mapping predicting the vorticity at a later point in time.

We represent the physics operator  $\mathcal{P}(\mathbf{x})$  by an FNO network. Since the turbulence simulation is deterministic,  $\Delta t$  is large and FNOs tend to smoothen noise (by using a limited number of modes for the power spectrum in the spectral convolution layers), we split the physics and score update during training, cf. 3c. For the score network  $s_\theta(\mathbf{x}, t)$ , we use the same ResNet-based architecture as in section 4.1.

**Training** As a first step of our method, we train the physics model  $\mathcal{P}(\mathbf{x})$  using the multi step loss and sliding window training setup from the previous two experiments, but freeze the score to  $s_\theta(\mathbf{x}, t) \equiv 0$ . We denote this method by *Learned physics*.

As a second step, we train the time-dependent score  $s_\theta(\mathbf{x}, t)$  while freezing the physics model  $\mathcal{P}$ . This approach guarantees that any time-independent physics are captured by  $\mathcal{P}$  and  $s_\theta(\mathbf{x}, t)$  can focus on learning small improvements to  $\mathcal{P}$  as well as respond to possibly time-dependent data biases. Alternatively, we test how successfully we can train both the physics model and  $s_\theta(\mathbf{x}, t)$  at the same time. As the two components resemble the drift and score of the reverse-time SDE, this

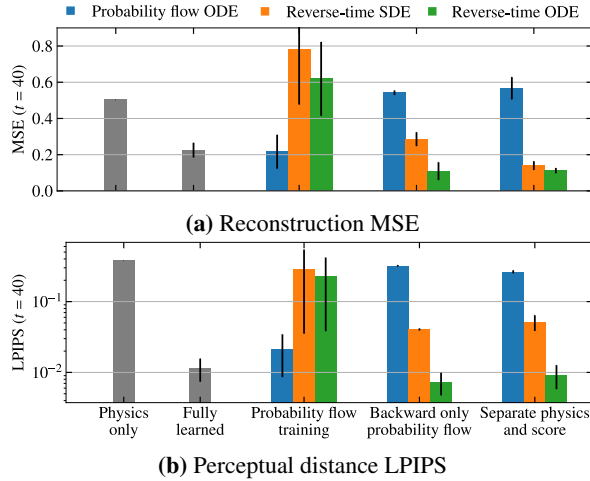


**Figure 9:** Evaluation of variants for the buoyancy obstacle case in terms of reconstruction MSE and LPIPS of the marker field. Averaged over 3 runs.

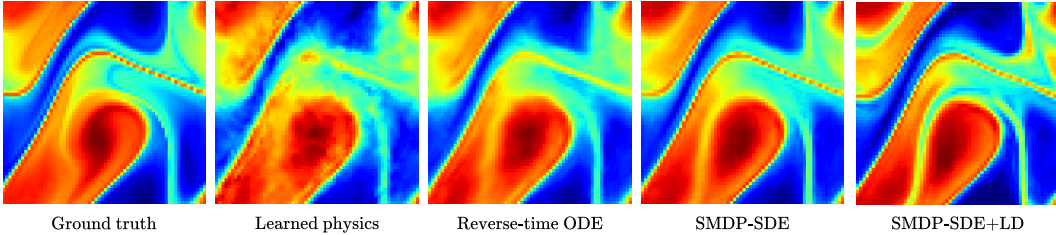


**Figure 10:** Turbulence case. Comparison of reconstructed trajectories at  $t = 9$ .

approach is similar to *DiffFlow* (Zhang & Chen, 2021), which learns both the score and optimal drift in the context of generative modeling. We label this approach *Combined training*.

**Evaluation** We evaluate the different methods in table 2. In this scenario, the *combined training* has severe difficulties to learn state updates and score field, resulting in large differences in terms of MSE. As before in section 4.1, the SMDP-SDE method performs best in terms of spectral error. Based on the results in section 4.2, we consider the reverse-time ODE for inference instead of SMDP-

Method	MSE $\downarrow$ [ $10^{-2}$ ]	Spectral Error $\downarrow$
Reverse-time ODE	<b>14.3</b>	0.26
SMDP-SDE	15.3	<b>0.17</b>
Combined training	221.2	0.58
Learned physics	16.3	0.30

**Table 2:** Evaluation of the turbulence case.

ODE. Compared to the *learned physics* variant, this improves the mean squared error (MSE) between the ground truth trajectories and the reconstructed trajectories slightly, while there is a substantial decrease in the spectral error. This can be seen qualitatively in figure 10.

**Outlook: Refinement with Langevin dynamics** Since the score  $\nabla_{\mathbf{x}} \log p_t(\mathbf{x})$  represents a data gradient, we can use gradient-based optimization methods to find local optima of the data distribution  $p_t(\mathbf{x})$  that are close to  $\mathbf{x}$ . Inspired by stochastic gradient Langevin dynamics (Welling & Teh, 2011), we consider the iteration rule  $\mathbf{x}_t^{i+1} = \mathbf{x}_t^i + \epsilon \cdot \nabla_{\mathbf{x}} \log p_t(\mathbf{x}_t^i) + \sqrt{2\epsilon}z_t$ , for  $\epsilon = 2 \times 10^{-5}$ , where  $z_t \sim \mathcal{N}(0, I)$  (details in appendix G.1). Denoted by *SMDP-SDE+LD* in figure 10, this method manages to generate even finer details from the reverse-time SDE solution. As such it provides an interesting starting point for a further refinement of the SMDP results.

## 5 CONCLUSION

We presented SMDP, a derivative of score matching in the context of physical simulations and differentiable physics. We showed its competitiveness against different baseline methods and in challenging inverse physics problems. We demonstrated the versatility of SMDP with two main approaches: while the *neural ODE* variants focus on high MSE accuracies, the *neural SDE* variants allow for sampling the posterior and yield an improved coverage of the target data manifold. We additionally provided new theoretical insights how the single step probability flow directly relates to optimizing the score matching objective, and how extending it to multiple steps can be seen as maximizing a variational lower bound for maximum likelihood training.

Despite the promising initial results, our work gives rise to many interesting questions. In particular, the time discretization is a crucial issue, as for training data generation and differentiable solvers, we would favor larger step size and less evaluations due to computational constraints, while for conventional diffusion models, a large number of smaller time steps often yields substantial improvements in terms of quality. Determining a good balance between accurate solutions with few time steps and diverse solutions with many time steps will remain an important direction for future research in this area.

---

## REFERENCES

- Brian Anderson. Reverse-time diffusion equation models. *Stochastic Processes and their Applications*, 12(3):313–326, 1982.
- Arpit Bansal, Eitan Borgnia, Hong-Min Chu, Jie S. Li, Hamid Kazemi, Furong Huang, Micah Goldblum, Jonas Geiping, and Tom Goldstein. Cold diffusion: Inverting arbitrary image transforms without noise. *CoRR*, abs/2208.09392, 2022. doi: 10.48550/arXiv.2208.09392. URL <https://doi.org/10.48550/arXiv.2208.09392>.
- Xavier Blanc, Claude Le Bris, and P-L Lions. From molecular models to continuum mechanics. *Archive for Rational Mechanics and Analysis*, 164(4):341–381, 2002.
- Johannes Brandstetter, Daniel Worrall, and Max Welling. Message passing neural pde solvers. *International Conference on Learning Representations*, 2022.
- Nanxin Chen, Yu Zhang, Heiga Zen, Ron J. Weiss, Mohammad Norouzi, and William Chan. Wavegrad: Estimating gradients for waveform generation. In *9th International Conference on Learning Representations, ICLR 2021, Virtual Event, Austria, May 3-7, 2021*. OpenReview.net, 2021. URL <https://openreview.net/forum?id=NsMLjcFa080>.
- Tian Qi Chen, Yulia Rubanova, Jesse Bettencourt, and David Duvenaud. Neural ordinary differential equations. In *Advances in Neural Information Processing Systems 31: Annual Conference on Neural Information Processing Systems 2018, NeurIPS 2018, December 3-8, 2018, Montréal, Canada*, pp. 6572–6583, 2018. URL <https://proceedings.neurips.cc/paper/2018/hash/69386f6bb1dfed68692a24c8686939b9-Abstract.html>.
- Hyungjin Chung, Byeongsu Sim, and Jong Chul Ye. Come-closer-diffuse-faster: Accelerating conditional diffusion models for inverse problems through stochastic contraction. *CoRR*, abs/2112.05146, 2021. URL <https://arxiv.org/abs/2112.05146>.
- Hyungjin Chung, Byeongsu Sim, Dohoon Ryu, and Jong Chul Ye. Improving diffusion models for inverse problems using manifold constraints. *CoRR*, abs/2206.00941, 2022. doi: 10.48550/arXiv.2206.00941. URL <https://doi.org/10.48550/arXiv.2206.00941>.
- Patrick R. Conrad, Mark A. Girolami, Simo Särkkä, Andrew M. Stuart, and Konstantinos Zygalakis. Statistical analysis of differential equations: introducing probability measures on numerical solutions. *Stat. Comput.*, 27(4):1065–1082, 2017. doi: 10.1007/s11222-016-9671-0. URL <https://doi.org/10.1007/s11222-016-9671-0>.
- S Delaquis, MJ Jewell, I Ostrovskiy, M Weber, T Ziegler, J Dalmasson, LJ Kaufman, T Richards, JB Albert, G Anton, et al. Deep neural networks for energy and position reconstruction in exo-200. *Journal of Instrumentation*, 13(08):P08023, 2018.
- Prafulla Dhariwal and Alexander Quinn Nichol. Diffusion models beat gans on image synthesis. In *Advances in Neural Information Processing Systems 34: Annual Conference on Neural Information Processing Systems 2021, NeurIPS 2021, December 6-14, 2021, virtual*, pp. 8780–8794, 2021. URL <https://proceedings.neurips.cc/paper/2021/hash/49ad23d1ec9fa4bd8d77d02681df5cfa-Abstract.html>.
- John Duchi. Derivations for linear algebra and optimization. *Berkeley, California*, 3(1):2325–5870, 2007.
- Stanley J Farlow. *Partial differential equations for scientists and engineers*. Courier Corporation, 1993.
- Rafael Gómez-Bombarelli, Jennifer N Wei, David Duvenaud, José Miguel Hernández-Lobato, Benjamín Sánchez-Lengeling, Dennis Sheberla, Jorge Aguilera-Iparraguirre, Timothy D Hirzel, Ryan P Adams, and Alán Aspuru-Guzik. Automatic chemical design using a data-driven continuous representation of molecules. *ACS central science*, 4(2):268–276, 2018.

- 
- Will Grathwohl, Ricky T. Q. Chen, Jesse Bettencourt, Ilya Sutskever, and David Duvenaud. FFJORD: free-form continuous dynamics for scalable reversible generative models. In *7th International Conference on Learning Representations, ICLR 2019, New Orleans, LA, USA, May 6-9, 2019*. OpenReview.net, 2019. URL <https://openreview.net/forum?id=rJxgknCcK7>.
- Morton E Gurtin. *An introduction to continuum mechanics*. Academic press, 1982.
- Jonathan Ho, Ajay Jain, and Pieter Abbeel. Denoising diffusion probabilistic models. In *Advances in Neural Information Processing Systems 33: Annual Conference on Neural Information Processing Systems 2020, NeurIPS 2020, December 6-12, 2020, virtual*, 2020. URL <https://proceedings.neurips.cc/paper/2020/hash/4c5bcfec8584af0d967f1ab10179ca4b-Abstract.html>.
- Jonathan Ho, Tim Salimans, Alexey A. Gritsenko, William Chan, Mohammad Norouzi, and David J. Fleet. Video diffusion models. *CoRR*, abs/2204.03458, 2022. doi: 10.48550/arXiv.2204.03458. URL <https://doi.org/10.48550/arXiv.2204.03458>.
- Philipp Holl, Vladlen Koltun, Kiwon Um, and Nils Thuerey. phiflow: A differentiable pde solving framework for deep learning via physical simulations. In *NeurIPS Workshop*, volume 2, 2020a.
- Philipp Holl, Nils Thuerey, and Vladlen Koltun. Learning to control pdes with differentiable physics. In *8th International Conference on Learning Representations, ICLR 2020, Addis Ababa, Ethiopia, April 26-30, 2020*. OpenReview.net, 2020b. URL <https://openreview.net/forum?id=HyeSin4FPB>.
- Tobias H"oppe, Arash Mehrjou, Stefan Bauer, Didrik Nielsen, and Andrea Dittadi. Diffusion models for video prediction and infilling. *CoRR*, abs/2206.07696, 2022. doi: 10.48550/arXiv.2206.07696. URL <https://doi.org/10.48550/arXiv.2206.07696>.
- Chin-Wei Huang, Jae Hyun Lim, and Aaron C. Courville. A variational perspective on diffusion-based generative models and score matching. In Marc'Aurelio Ranzato, Alina Beygelzimer, Yann N. Dauphin, Percy Liang, and Jennifer Wortman Vaughan (eds.), *Advances in Neural Information Processing Systems 34: Annual Conference on Neural Information Processing Systems 2021, NeurIPS 2021, December 6-14, 2021, virtual*, pp. 22863–22876, 2021. URL <https://proceedings.neurips.cc/paper/2021/hash/c11labfd29e4d9b4d4b566b01114d8486-Abstract.html>.
- Aapo Hyv"arinen. Estimation of non-normalized statistical models by score matching. *J. Mach. Learn. Res.*, 6:695–709, 2005. URL <http://jmlr.org/papers/v6/hyvarinen05a.html>.
- Alexia Jolicoeur-Martineau, Ke Li, R"emi Pich"e-Taillefer, Tal Kachman, and Ioannis Mitliagkas. Gotta go fast when generating data with score-based models. *arXiv preprint arXiv:2105.14080*, 2021.
- Bahjat Kawar, Gregory Vaksman, and Michael Elad. SNIPS: solving noisy inverse problems stochastically. In *Advances in Neural Information Processing Systems 34: Annual Conference on Neural Information Processing Systems 2021, NeurIPS 2021, December 6-14, 2021, virtual*, pp. 21757–21769, 2021. URL <https://proceedings.neurips.cc/paper/2021/hash/b5c01503041b70d41d80e3dbe31bbd8c-Abstract.html>.
- Hans Kersting, Nicholas Kr"amer, Martin Schiegg, Christian Daniel, Michael Tiemann, and Philipp Hennig. Differentiable likelihoods for fast inversion of 'likelihood-free' dynamical systems. In *Proceedings of the 37th International Conference on Machine Learning, ICML 2020, 13-18 July 2020, Virtual Event*, volume 119 of *Proceedings of Machine Learning Research*, pp. 5198–5208. PMLR, 2020. URL <http://proceedings.mlr.press/v119/kersting20a.html>.
- Dmitrii Kochkov, Jamie A. Smith, Ayya Alieva, Qing Wang, Michael P. Brenner, and Stephan Hoyer. Machine learning accelerated computational fluid dynamics. *CoRR*, abs/2102.01010, 2021. URL <https://arxiv.org/abs/2102.01010>.

- 
- Sizhe Li, Zhiao Huang, Tao Du, Hao Su, Joshua B Tenenbaum, and Chuang Gan. Contact points discovery for soft-body manipulations with differentiable physics. *International Conference on Learning Representations*, 2022.
- Zongyi Li, Nikola Kovachki, Kamyar Azizzadenesheli, Burigede Liu, Kaushik Bhattacharya, Andrew Stuart, and Anima Anandkumar. Fourier neural operator for parametric partial differential equations. *arXiv:2010.08895*, 2020.
- Joowon Lim and Demetri Psaltis. Maxwellnet: Physics-driven deep neural network training based on maxwell’s equations. *Apl Photonics*, 7(1):011301, 2022.
- Cheng Lu, Kaiwen Zheng, Fan Bao, Jianfei Chen, Chongxuan Li, and Jun Zhu. Maximum likelihood training for score-based diffusion odes by high order denoising score matching. In *International Conference on Machine Learning, ICML 2022, 17-23 July 2022, Baltimore, Maryland, USA*, volume 162 of *Proceedings of Machine Learning Research*, pp. 14429–14460. PMLR, 2022. URL <https://proceedings.mlr.press/v162/lu22f.html>.
- Dimitra Maoutsa, Sebastian Reich, and Manfred Opper. Interacting particle solutions of fokker-planck equations through gradient-log-density estimation. *Entropy*, 22(8):802, 2020. doi: 10.3390/e22080802. URL <https://doi.org/10.3390/e22080802>.
- Glenn J Martyna, Mark E Tuckerman, Douglas J Tobias, and Michael L Klein. Explicit reversible integrators for extended systems dynamics. *Molecular Physics*, 87(5):1117–1157, 1996.
- Jeremy Morton, Antony Jameson, Mykel J Kochenderfer, and Freddie Witherden. Deep dynamical modeling and control of unsteady fluid flows. In *Advances in Neural Information Processing Systems*, 2018.
- Maximilian Mueller, Robin Greif, Frank Jenko, and Nils Thuerey. Leveraging stochastic predictions of bayesian neural networks for fluid simulations. *arXiv preprint arXiv:2205.01222*, 2022.
- Bernt Øksendal. Stochastic differential equations. In *Stochastic differential equations*, pp. 65–84. Springer, 2003.
- Tobias Pfaff, Meire Fortunato, Alvaro Sanchez-Gonzalez, and Peter Battaglia. Learning mesh-based simulation with graph networks. *International Conference on Learning Representations*, 2020.
- Zacharie Ramzi, Benjamin Remy, François Lanusse, Jean-Luc Starck, and Philippe Ciuciu. Denoising score-matching for uncertainty quantification in inverse problems. *CoRR*, abs/2011.08698, 2020. URL <https://arxiv.org/abs/2011.08698>.
- Severi Rissanen, Markus Heinonen, and Arno Solin. Generative modelling with inverse heat dissipation. *arXiv:2206.13397*, 2022.
- Samuel Schoenholz and Ekin Dogus Cubuk. Jax md: a framework for differentiable physics. *Advances in Neural Information Processing Systems*, 33:11428–11441, 2020.
- Jascha Sohl-Dickstein, Eric A. Weiss, Niru Maheswaranathan, and Surya Ganguli. Deep unsupervised learning using nonequilibrium thermodynamics. In *Proceedings of the 32nd International Conference on Machine Learning, ICML 2015, Lille, France, 6-11 July 2015*, volume 37 of *JMLR Workshop and Conference Proceedings*, pp. 2256–2265. JMLR.org, 2015. URL <http://proceedings.mlr.press/v37/sohl-dickstein15.html>.
- Yang Song and Stefano Ermon. Generative modeling by estimating gradients of the data distribution. In *Advances in Neural Information Processing Systems 32: Annual Conference on Neural Information Processing Systems 2019, NeurIPS 2019, December 8-14, 2019, Vancouver, BC, Canada*, pp. 11895–11907, 2019. URL <https://proceedings.neurips.cc/paper/2019/hash/3001ef257407d5a371a96dcd947c7d93-Abstract.html>.
- Yang Song, Conor Durkan, Iain Murray, and Stefano Ermon. Maximum likelihood training of score-based diffusion models. In *Advances in Neural Information Processing Systems 34: Annual Conference on Neural Information Processing Systems 2021, NeurIPS 2021, December 6-14, 2021, virtual*, pp. 1415–1428, 2021a. URL <https://proceedings.neurips.cc/paper/2021/hash/0a9fdbb17feb6ccb7ec405cfb85222c4-Abstract.html>.



- 
- Yang Song, Liyue Shen, Lei Xing, and Stefano Ermon. Solving inverse problems in medical imaging with score-based generative models. *CoRR*, abs/2111.08005, 2021b. URL <https://arxiv.org/abs/2111.08005>.
- Yang Song, Jascha Sohl-Dickstein, Diederik P. Kingma, Abhishek Kumar, Stefano Ermon, and Ben Poole. Score-based generative modeling through stochastic differential equations. In *9th International Conference on Learning Representations, ICLR 2021, Virtual Event, Austria, May 3-7, 2021*. OpenReview.net, 2021c. URL <https://openreview.net/forum?id=PXTIG12RRHS>.
- Kim Stachenfeld, Drummond Buschman Fielding, Dmitrii Kochkov, Miles Cranmer, Tobias Pfaff, Jonathan Godwin, Can Cui, Shirley Ho, Peter Battaglia, and Alvaro Sanchez-Gonzalez. Learned simulators for turbulence. In *International Conference on Learning Representations, 2021*.
- Jonathan Tompson, Kristofer Schlachter, Pablo Sprechmann, and Ken Perlin. Accelerating eulerian fluid simulation with convolutional networks. In *5th International Conference on Learning Representations, ICLR 2017, Toulon, France, April 24-26, 2017, Workshop Track Proceedings*. OpenReview.net, 2017. URL <https://openreview.net/forum?id=ByH2gxrKl>.
- Kiwon Um, Robert Brand, Yun (Raymond) Fei, Philipp Holl, and Nils Thuerey. Solver-in-the-loop: Learning from differentiable physics to interact with iterative pde-solvers. In *Advances in Neural Information Processing Systems 33: Annual Conference on Neural Information Processing Systems 2020, NeurIPS 2020, December 6-12, 2020, virtual, 2020*. URL <https://proceedings.neurips.cc/paper/2020/hash/43e4e6a6f341e00671e123714de019a8-Abstract.html>.
- Pascal Vincent. A connection between score matching and denoising autoencoders. *Neural Comput.*, 23(7):1661–1674, 2011. doi: 10.1162/NECO\\_a\\_.00142. URL [https://doi.org/10.1162/NECO\\_a\\_00142](https://doi.org/10.1162/NECO_a_00142).
- Max Welling and Yee Whye Teh. Bayesian learning via stochastic gradient langevin dynamics. In Lise Getoor and Tobias Scheffer (eds.), *Proceedings of the 28th International Conference on Machine Learning, ICML 2011, Bellevue, Washington, USA, June 28 - July 2, 2011*, pp. 681–688. Omnipress, 2011. URL [https://icml.cc/2011/papers/398\\_icmlpaper.pdf](https://icml.cc/2011/papers/398_icmlpaper.pdf).
- Ruihan Yang, Prakhar Srivastava, and Stephan Mandt. Diffusion probabilistic modeling for video generation. *CoRR*, abs/2203.09481, 2022. doi: 10.48550/arXiv.2203.09481. URL <https://doi.org/10.48550/arXiv.2203.09481>.
- Qinsheng Zhang and Yongxin Chen. Diffusion normalizing flow. *Advances in Neural Information Processing Systems*, 34:16280–16291, 2021.
- Richard Zhang, Phillip Isola, Alexei A Efros, Eli Shechtman, and Oliver Wang. The unreasonable effectiveness of deep features as a perceptual metric. In *Proceedings of the IEEE conference on computer vision and pattern recognition*, pp. 586–595, 2018.
- Kemin Zhou, JC Doyle, and Keither Glover. Robust and optimal control. *Control Engineering Practice*, 4(8):1189–1190, 1996.

---

## APPENDIX

### A DERIVATION OF TRAINING METHODOLOGY

Below we summarize the problem formulation from the main paper, and provide details about the training procedure and the derivation of our methodology.

**Problem setting** We consider the time evolution of the physical system modeled by the stochastic differential equation

$$d\mathbf{x} = \mathcal{P}(\mathbf{x})dt + g(t)dw, \quad (14)$$

with a drift  $\mathcal{P} : \mathbb{R}^d \rightarrow \mathbb{R}^d$  and diffusion  $g : [0, T] \rightarrow \mathbb{R}^+$ , which transforms the marginal distribution  $p_0$  of initial states at time 0 to the marginal distribution  $p_T$  of end states at time  $T$ . Moreover, we assume that we have sampled  $N$  trajectories of length  $M$  from the above SDE with a fixed time discretization  $0 \leq t_0 < t_1 < \dots < t_M \leq T$  for the interval  $[0, T]$  and collected them in a training data set  $\{\mathbf{x}_{t_i, n}\}_{i=0, \dots, M}^{n=0, \dots, N}$ .

We are interested in training a neural network  $s_\theta(\mathbf{x}, t)$  parameterized by  $\theta$  to approximate the score  $\nabla_{\mathbf{x}} \log p_t(\mathbf{x})$ , i.e. minimize the score matching objective

$$\mathcal{J}_{\text{SM}}(\theta; \lambda(\cdot)) := \frac{1}{2} \int_0^T \mathbb{E}_{\mathbf{x} \sim p_t} \left[ \lambda(t) \|\mathbf{s}_\theta(\mathbf{x}, t) - \nabla_{\mathbf{x}} \log p_t(\mathbf{x})\|_2^2 \right] dt, \quad (15)$$

where  $\lambda : [0, T] \mapsto \mathbb{R}^+$  is a weighting function. In the case of denoising score matching, where the underlying SDE is  $d\mathbf{x} = f(\mathbf{x}, t)dt + g(t)dw$  for affine functions  $f(\cdot)$  and  $g(\cdot)$ , the score can be learned by minimizing the denoising score matching objective using transition kernels, which enables an efficient training of diffusion models, see Song et al. (2021c) for a reference.

In our case,  $\mathcal{P}$  is an arbitrary function describing the dynamics of the physical system, and hence we can not rely on an analytical expression for the transition kernel.

#### A.1 TRAINING VIA CONTINUOUS NORMALIZING FLOWS

Score-based diffusion models can be transformed into continuous normalizing flows (Chen et al., 2018, CNFs), which allows for a tractable computation of the likelihood. We can train the corresponding CNF given by

$$d\mathbf{x} = \left[ \mathcal{P}(\mathbf{x}) - \frac{1}{2}g^2(t)s_\theta(\mathbf{x}, t) \right] dt \quad (16)$$

using maximum likelihood training, i.e. maximizing

$$\mathbb{E}_{\mathbf{x}_0 \sim p_0} [\log p_0^{\text{ODE}}(\mathbf{x}_0)] \quad (17)$$

$$\text{s.t. } \mathbf{x}_T = \mathbf{x}_0 + \int_0^T \left[ \mathcal{P}(\mathbf{x}_t) - \frac{1}{2}g^2(t)s_\theta(\mathbf{x}_t, t) \right] dt, \quad (18)$$

where  $p_0^{\text{ODE}}$  is the distribution obtained by sampling  $\mathbf{x}_T \sim p_T$  and simulating  $\mathbf{x}_0$  using ODE equation (16). The log-likelihood can be computed using the instantaneous change of variables formula (Chen et al., 2018) and by using the fact that  $p_T$  is approximately Gaussian.

The maximum likelihood training can also be written in terms of the Kullback-Leibler divergence, i.e. instead of maximizing equation (16), we can equivalently minimize

$$\text{KL}(p_0 \parallel p_0^{\text{ODE}}). \quad (19)$$

For denoising score matching, maximum likelihood training of the corresponding CNF is typically not used, because it requires running an ODE solver for every optimization step and the training with the denoising score matching objective is more efficient (Huang et al., 2021; Song et al., 2021a). It was shown by Song et al. (2021a) that there is connection between the Kullback-Leibler divergence and the score matching objective. In particular

$$\text{KL}(p_0 \parallel p_\theta^{\text{SDE}}) \leq \mathcal{J}_{\text{SM}}(\theta; g(\cdot)^2) + \text{KL}(p_T \parallel \pi) \quad (20)$$

for a prior distribution  $\pi$  and  $p_\theta^{\text{SDE}}$  defined by sampling  $\mathbf{x}_T \sim \pi$  and solving the reverse-time SDE using the score approximation  $s_\theta(\mathbf{x}, t)$ .

## A.2 SINGLE STEPS

In this section, we consider the single step loss

$$\mathcal{L}_{\text{single}}(\theta) = \mathbb{E}_{(\mathbf{x}_{t_{i-1}}, \mathbf{x}_{t_i}, \mathbf{x}_{t_{i+1}})} \left[ \|\mathbf{x}_{t_{i+1}} - \mu_{t_{i+1}}^{\text{ODE,F}}(\mathbf{x}_{t_i})\|_2^2 + \|\mathbf{x}_{t_{i-1}} - \mu_{t_{i-1}}^{\text{ODE,B}}(\mathbf{x}_{t_i})\|_2^2 \right], \quad (21)$$

where  $\mu_{t_{i+1}}^{\text{ODE,F}}(\mathbf{x}_{t_i})$  is obtained by integrating the probability flow ODE with score representation

$$d\mathbf{x} = \left[ \mathcal{P}(\mathbf{x}) - \frac{1}{2}g(t)^2 s_\theta(\mathbf{x}, t) \right] dt \quad (22)$$

given the sample  $\mathbf{x}_{t_i}$  at time  $t_i$  forwards in time until  $t_{i+1}$ . Analogously, for  $\mu_{t_{i-1}}^{\text{ODE,B}}(\mathbf{x}_{t_i})$ , the probability flow ODE with score representation is integrated backward from time  $t_i$  to  $t_{i-1}$ . We show that the single step loss equation (21) is an unbiased estimator (up to a constant factor) for the sum of the two Kullback-Leibler divergences

$$\text{KL}(p_{t_{i-1}} \times p_{t_i} \| p_{t_{i-1}}^{t_i, \text{ODE}} \times p_{t_i}) + \text{KL}(p_{t_i} \times p_{t_{i+1}} \| p_{t_i} \times p_{t_{i+1}}^{t_i, \text{ODE}}), \quad (23)$$

where  $p_{t_{i-1}}^{t_i, \text{ODE}}$  is obtained by sampling  $\mathbf{x} \sim p_{t_i}$  and integrating the probability flow with network  $s_\theta(\mathbf{x}, t)$  equation equation (22) backward in time until  $t_{i-1}$  and analogously for  $p_{t_{i+1}}^{t_i, \text{ODE}}$ . The term  $p_{t_i} \times p_{t_{i+1}}$  refers to the joint distribution of data pairs at time  $t_i$  and  $t_{i+1}$ , which has  $p_{t_i}$  and  $p_{t_{i+1}}$  as marginals. For the three time steps  $t_{i-1}, t_i$  and  $t_{i+1}$  minimizing the sum of KL-divergences equation (23) can be regarded as a maximum likelihood training, similar to the maximum likelihood training of the continuous normalizing flows discussed in section A.1. However, in this case we show that for small  $\Delta t$ , this directly relates to the score matching objective equation (3).

First, we show that under the assumption that  $\Delta t$  is small, the KL-divergence objective equation (23) is minimized when  $s_\theta(\mathbf{x}, t) \equiv \nabla_{\mathbf{x}} \log p_t(\mathbf{x})$ .

We rewrite equation (23) as

$$\text{KL}(p_{t_{i-1}} \times p_{t_i} \| p_{t_{i-1}}^{t_i, \text{ODE}} \times p_{t_i}) + \text{KL}(p_{t_i} \times p_{t_{i+1}} \| p_{t_i} \times p_{t_{i+1}}^{t_i, \text{ODE}}) \quad (24)$$

$$= \mathbb{E}_{(\mathbf{x}_{t_{i-1}}, \mathbf{x}_{t_i})} \left[ \log \frac{p_{t_{i-1}}(\mathbf{x}_{t_{i-1}}, \mathbf{x}_{t_i}) p(\mathbf{x}_{t_i})}{p_{t_{i-1}}^{t_i, \text{ODE}}(\mathbf{x}_{t_{i-1}} | \mathbf{x}_{t_i}) p(\mathbf{x}_{t_i})} \right] \quad (25)$$

$$+ \mathbb{E}_{(\mathbf{x}_t, \mathbf{x}_{t_{i+1}})} \left[ \log \frac{p_{t_i}(\mathbf{x}_{t_{i+1}} | \mathbf{x}_{t_i}) p(\mathbf{x}_{t_i})}{p_{t_{i+1}}^{t_i, \text{ODE}}(\mathbf{x}_{t_{i+1}} | \mathbf{x}_{t_i}) p(\mathbf{x}_{t_i})} \right] \quad (26)$$

$$= \mathbb{E}_{\mathbf{x}_{t_i}} \mathbb{E}_{\mathbf{x}_{t_{i-1}} | \mathbf{x}_{t_i}} \left[ \log \frac{p_{t_{i-1}}(\mathbf{x}_{t_{i-1}} | \mathbf{x}_{t_i})}{p_{t_{i-1}}^{t_i, \text{ODE}}(\mathbf{x}_{t_{i-1}} | \mathbf{x}_{t_i})} \right] \quad (27)$$

$$+ \mathbb{E}_{\mathbf{x}_{t_i}} \mathbb{E}_{\mathbf{x}_{t_{i+1}} | \mathbf{x}_{t_i}} \left[ \log \frac{p_{t_i}(\mathbf{x}_{t_{i+1}} | \mathbf{x}_{t_i})}{p_{t_{i+1}}^{t_i, \text{ODE}}(\mathbf{x}_{t_{i+1}} | \mathbf{x}_{t_i})} \right] \quad (28)$$

$$= \mathbb{E}_{\mathbf{x}_{t_i}} \left[ \text{KL}(p_{t_{i-1}} | \mathbf{x}_{t_i} \| p_{t_{i-1}}^{t_i, \text{ODE}} | \mathbf{x}_{t_i}) + \text{KL}(p_{t_{i+1}} | \mathbf{x}_{t_i} \| p_{t_{i+1}}^{t_i, \text{ODE}} | \mathbf{x}_{t_i}) \right]. \quad (29)$$

We make the simplifying assumption that  $t_i - t_{i-1} = t_{i+1} - t_i := \Delta t$ . Then, if  $\Delta t$  is small, with Euler-Maruyama steps we can use the SDE of the physical system equation equation (5) and the reverse-time SDE equation (7) to approximate

$$\mathbf{x}_{t_{i+1}} = \mathbf{x}_{t_i} + \Delta t \mathcal{P}(\mathbf{x}_{t_i}) + \sqrt{\Delta t} g(t_i) z_{t_i} \quad (30)$$

$$\mathbf{x}_{t_{i-1}} = \mathbf{x}_{t_i} - \Delta t [\mathcal{P}(\mathbf{x}_{t_i}) - g(t_i)^2 \nabla_{\mathbf{x}} \log p_{t_i}] + \sqrt{\Delta t} g(t_i) z'_{t_i}, \quad (31)$$

where  $z_{t_i}$  and  $z'_{t_i}$  are drawn from a normal Gaussian distribution. Thus, the distributions  $p_{t_{i-1}} | \mathbf{x}_{t_i}$  and  $p_{t_{i+1}} | \mathbf{x}_{t_i}$  can be modeled as Gaussian distributions with mean given by the first two terms in equation (30) and equation (31) and standard deviation  $\sigma = \sqrt{\Delta t} g(t_i)$ .

Additionally, to apply methods for variational inference, we want to model the deterministic ODE solutions  $p_{t_{i-1}}^{t_i, \text{ODE}} | \mathbf{x}_{t_i}$  and  $p_{t_{i+1}}^{t_i, \text{ODE}} | \mathbf{x}_{t_i}$  as distributions. For this purpose, we consider Gaussian

ODE filtering (Kersting et al., 2020). Using a single Euler step, we can represent the conditional distributions as Gaussian distributions with means

$$\mu_{t_{i-1}}^{t_i, \text{ODE}}(\mathbf{x}_{t_i}) = \mathbf{x}_{t_i} - \Delta t \left[ \mathcal{P}(\mathbf{x}_t) - \frac{1}{2}g(t_i)^2 s_\theta(\mathbf{x}_{t_i}, t_i) \right] \quad (32)$$

$$\mu_{t_{i+1}}^{t_i, \text{ODE}}(\mathbf{x}_{t_i}) = \mathbf{x}_{t_i} + \Delta t \left[ \mathcal{P}(\mathbf{x}_t) - \frac{1}{2}g(t_i)^2 s_\theta(\mathbf{x}_{t_i}, t_i) \right]. \quad (33)$$

and variance  $\sigma^2 = \epsilon$  for a fixed  $\epsilon > 0$ , that represents a Laplace approximation (Conrad et al., 2017) of the errors introduced by the Euler step.

The KL-divergence terms for multivariate Gaussian distributions can be computed analytically, see e.g. Duchi (2007, Chapter 13). For two multivariate Gaussian distributions  $P$  and  $Q$  with

$$P \sim \mathcal{N}(\mu_1, \Sigma_1) \quad (34)$$

and

$$Q \sim \mathcal{N}(\mu_2, \Sigma_2), \quad (35)$$

the KL-divergence  $\text{KL}(P||Q)$  can be computed analytically as

$$\text{KL}(P||Q) = \frac{1}{2} \left[ (\mu_2 - \mu_1)^T \Sigma_2^{-1} (\mu_2 - \mu_1) + \text{tr}(\Sigma_2^{-1} \Sigma_1) - \log \left( \frac{|\Sigma_1|}{|\Sigma_2|} \right) - n \right]. \quad (36)$$

Therefore, we can simplify the two KL-divergence terms from equation (29) with

$$\text{KL}(p_{t_{i-1}}|\mathbf{x}_{t_i}||p_{t_{i-1}}^{\text{ODE}, t_i}|\mathbf{x}_{t_i}) \quad (37)$$

$$= \frac{1}{\epsilon^2} \|\mathbf{x}_{t_i} - \Delta t \left[ \mathcal{P}(\mathbf{x}_{t_i}) - g(t_i)^2 \nabla_{\mathbf{x}} \log p_{t_i}(\mathbf{x}_{t_i}) \right] - \mu_{t_{i-1}}^{t_i, \text{ODE}}(\mathbf{x}_{t_i})\|_2^2 + C_1 \quad (38)$$

$$= \frac{1}{\epsilon^2} \|\Delta t g(t_i)^2 \left[ \nabla_{\mathbf{x}} \log p_{t_i}(\mathbf{x}_{t_i}) - \frac{1}{2} s_\theta(\mathbf{x}_{t_i}, t_i) \right]\|_2^2 + C_1 \quad (39)$$

and

$$\text{KL}(p_{t_{i+1}}|\mathbf{x}_{t_i}||p_{t_{i+1}}^{\text{ODE}, t_i}|\mathbf{x}_{t_i}) \quad (40)$$

$$= \frac{1}{\epsilon^2} \|\mathbf{x}_{t_i} + \Delta t \mathcal{P}(\mathbf{x}_{t_i}) - \mu_{t_{i+1}}^{t_i, \text{ODE}}(\mathbf{x}_{t_i})\|_2^2 + C_2 \quad (41)$$

$$= \frac{1}{\epsilon^2} \|\Delta t g(t_i)^2 \frac{1}{2} s_\theta(\mathbf{x}_{t_i}, t_i)\|_2^2 + C_2 \quad (42)$$

with  $C_1$  and  $C_2$  are constants independent of  $\theta$  and  $\mathbf{x}_{t_i}$ . Thus, the minimizer for equation (29) equally minimizes

$$\frac{1}{\epsilon^2} \Delta t^2 g(t_i)^4 \mathbb{E}_{\mathbf{x}_{t_i}} \left[ \|\nabla_{\mathbf{x}} \log p_{t_i}(\mathbf{x}_{t_i}) - \frac{1}{2} s_\theta(\mathbf{x}_{t_i}, t_i)\|_2^2 + \|\frac{1}{2} s_\theta(\mathbf{x}_{t_i}, t_i)\|_2^2 \right]. \quad (43)$$

To find the minima of equation (43), we consider the more general problem

$$\arg \min_{\mathbf{b} \in \mathbb{R}^n} \|\mathbf{a} - \mathbf{b}\|_2^2 + \|\mathbf{b}\|_2^2 \quad (44)$$

for a given  $\mathbf{a} \in \mathbb{R}^n$ . Taking the derivatives of the expressions in equation (44) with respect to  $\mathbf{b}$  and setting it to zero, we obtain

$$2(\mathbf{b} - \mathbf{a}) + 2\mathbf{b} = 0 \quad (45)$$

$$\Leftrightarrow \mathbf{b} = \frac{1}{2}\mathbf{a}. \quad (46)$$

Therefore  $\mathbf{b} = \frac{1}{2}\mathbf{a}$  is a minimizer of equation (44). By pointwise matching  $s_\theta(\mathbf{x}_{t_i}, t_i)$  and  $\nabla_{\mathbf{x}} \log p_{t_i}(\mathbf{x}_{t_i})$ , equation (43) is minimized when

$$\frac{1}{2} s_\theta(\mathbf{x}_{t_i}, t_i) = \frac{1}{2} \nabla_{\mathbf{x}} \log p_{t_i}(\mathbf{x}_{t_i}) \quad (47)$$

and therefore

$$s_\theta(\mathbf{x}_{t_i}, t_i) = \nabla_{\mathbf{x}} \log p_{t_i}(\mathbf{x}_{t_i}). \quad (48)$$

Note that this is true independent of  $\epsilon > 0$  from the Laplace approximation.

Finally, we show that we can estimate equation (43) (up to a constant factor) via the single step loss  $\mathcal{L}_{\text{single}}(\theta)$

$$\Delta t^2 g(t_i)^4 \mathbb{E}_{\mathbf{x}_{t_i}} \left[ \|\nabla_{\mathbf{x}} \log p_{t_i}(\mathbf{x}_{t_i}) - \frac{1}{2} s_{\theta}(\mathbf{x}_{t_i}, t_i)\|_2^2 + \|\frac{1}{2} s_{\theta}(\mathbf{x}_{t_i}, t_i)\|_2^2 \right] \quad (49)$$

$$= \mathbb{E}_{\mathbf{x}_{t_i}} \left[ \mathbb{E}_{\mathbf{x}_{t_{i-1}}|\mathbf{x}_{t_i}} \left[ \|\mathbf{x}_{t_{i-1}} - \mu_{t_{i-1}}^{t_i, \text{ODE}}(\mathbf{x}_{t_i})\|_2^2 \right] + \mathbb{E}_{\mathbf{x}_{t_{i+1}}|\mathbf{x}_{t_i}} \left[ \|\mathbf{x}_{t_{i+1}} - \mu_{t_{i+1}}^{t_i, \text{ODE}}(\mathbf{x}_{t_i})\|_2^2 \right] \right] \quad (50)$$

$$= \mathbb{E}_{(\mathbf{x}_{t_{i-1}}, \mathbf{x}_{t_i}, \mathbf{x}_{t_{i+1}})} \left[ \|\mathbf{x}_{t_{i-1}} - \mu_{t_{i-1}}^{t_i, \text{ODE}}(\mathbf{x}_{t_i})\|_2^2 + \|\mathbf{x}_{t_{i+1}} - \mu_{t_{i+1}}^{t_i, \text{ODE}}(\mathbf{x}_{t_i})\|_2^2 \right] \quad (51)$$

$$= \mathcal{L}_{\text{single}}(\theta). \quad (52)$$

It is also possible to compute the term  $\|s_{\theta}(\mathbf{x}_{t_i}, t_i)\|_2^2$  directly instead of estimating it using  $\|\mathbf{x}_{t_{i+1}} - \mu_{t_{i+1}}^{t_i, \text{ODE}}(\mathbf{x}_{t_i})\|_2^2$ . This way, it acts as a L2 regularization on the network output with weight  $\frac{1}{4} \Delta t^2 g(t_i)^4$ . We have not tested the effect of this on the training in the paper.

### A.3 MULTI STEP FORMULATION

We now extend the single step formulation from above to multiple steps. First, we consider the maximum likelihood training objective of the CNF discussed in section A.1. We can choose two arbitrary time points  $t_i$  and  $t_j$  with  $t_i > t_j$ , because we do not require to fix the simulation start and end times. Then, the objective equation (17) can be written as maximizing

$$\mathbb{E}_{\mathbf{x}_{t_i} \sim p_{t_i}} [\log p_{t_i}^{t_j, \text{ODE}}(\mathbf{x}_{t_i})] \quad (53)$$

$$\text{s.t. } \mathbf{x}_{t_i} = \mathbf{x}_{t_j} + \int_{t_i}^{t_j} \mathcal{P}(\mathbf{x}_t) - \frac{1}{2} g^2(t) s_{\theta}(\mathbf{x}_t, t) dt. \quad (54)$$

For this objective, we can derive a variational lower bound

$$\mathbb{E}_{\mathbf{x}_{t_i}} [\log p_{t_i}^{t_j, \text{ODE}}(\mathbf{x}_{t_i})] = \mathbb{E}_{\mathbf{x}_{t_i}} \left[ \log \left( \mathbb{E}_{\mathbf{x}_{t_j}} \left[ p_{t_i}^{t_j, \text{ODE}}(\mathbf{x}_{t_i} | \mathbf{x}_{t_j}) \right] \right) \right] \quad (55)$$

$$= \mathbb{E}_{\mathbf{x}_{t_i}} \left[ \log \left( \mathbb{E}_{\mathbf{x}_{t_j} | \mathbf{x}_{t_i}} \left[ \frac{p_{t_i}(\mathbf{x}_{t_i})}{p_{t_j}(\mathbf{x}_{t_j} | \mathbf{x}_{t_i})} p_{t_i}^{t_j, \text{ODE}}(\mathbf{x}_{t_i} | \mathbf{x}_{t_j}) \right] \right) \right] \quad (56)$$

$$\geq \mathbb{E}_{\mathbf{x}_{t_i}} \mathbb{E}_{\mathbf{x}_{t_j} | \mathbf{x}_{t_i}} \left[ \log \left( \frac{p_{t_j}(\mathbf{x}_{t_j})}{p_{t_j}(\mathbf{x}_{t_j} | \mathbf{x}_{t_i})} p_{t_i}^{t_j, \text{ODE}}(\mathbf{x}_{t_i} | \mathbf{x}_{t_j}) \right) \right] \quad (57)$$

$$= \mathbb{E}_{\mathbf{x}_{t_i}} \mathbb{E}_{\mathbf{x}_{t_j} | \mathbf{x}_{t_i}} \left[ \log \left( \frac{p_{t_j}(\mathbf{x}_{t_j})}{p_{t_j}(\mathbf{x}_{t_j} | \mathbf{x}_{t_i})} \right) + \log \left( p_{t_i}^{t_j, \text{ODE}}(\mathbf{x}_{t_i} | \mathbf{x}_{t_j}) \right) \right], \quad (58)$$

where the inequality is due to Jensen's inequality. This is the same as maximizing

$$\mathbb{E}_{\mathbf{x}_{t_i}} \mathbb{E}_{\mathbf{x}_{t_j} | \mathbf{x}_{t_i}} \left[ \log \left( p_{t_i}^{t_j, \text{ODE}}(\mathbf{x}_{t_i} | \mathbf{x}_{t_j}) \right) \right]. \quad (59)$$

Since this is true for any time step  $t_j > t_i$  and corresponding simulation state  $\mathbf{x}_{t_j}$ , given  $\mathbf{x}_{t_i}$ , we can pick the pairs  $(\mathbf{x}_{t_i}, \mathbf{x}_{t_{i+1}})$ ,  $(\mathbf{x}_{t_i}, \mathbf{x}_{t_{i+2}})$ ,  $(\mathbf{x}_{t_i}, \mathbf{x}_{t_{i+3}})$  and so on. Then, we can optimize them jointly by considering the sum of the individual objectives. Analogously to the single step formulation, we perturb the ODE distributions by convolving them with a Gaussian kernel  $G_{\epsilon}$  (Gaussian ODE filtering) and we model  $p_{t_i}^{t_j, \text{ODE}} | \mathbf{x}_{t_j}$  as a Gaussian distribution with mean  $\mu_{t_i}^{t_j, \text{ODE}}(\mathbf{x}_{t_j})$  and variance  $\sigma^2 := \epsilon > 0$ . Then maximizing equation (59) reduces to minimizing

$$\mathbb{E}_{\mathbf{x}_{t_i}} \mathbb{E}_{\mathbf{x}_{t_j} | \mathbf{x}_{t_i}} \left[ \|\mathbf{x}_{t_j} - \mu_{t_j}^{t_i, \text{ODE}}(\mathbf{x}_{t_i})\|_2^2 \right]. \quad (60)$$

By summing up the individual loss terms, we obtain the expression

$$\mathbb{E}_{(\mathbf{x}_{t_i}, \dots, \mathbf{x}_{t_j})} \left[ \sum_{k=i+1}^{j-1} \|\mathbf{x}_{t_k} - \mu_{t_k}^{t_i, \text{ODE}}(\mathbf{x}_{t_i})\|_2^2 \right]. \quad (61)$$

In our implementation, we do not compute the terms  $\mu_{t_k}^{t_i, \text{ODE}}(\mathbf{x}_{t_i})$  individually, but calculate them as part of the longest trajectory from  $t_i$  to  $t_j$ . Therefore, we obtain the multi step formulation for the forward direction

$$\mathbb{E}_{(\mathbf{x}_{t_i}, \dots, \mathbf{x}_{t_j})} \left[ \sum_{k=i+1}^{j-1} \|\mathbf{x}_{t_k} - \mathbf{x}_{t_k}^{\text{ODE}}(\mathbf{x}_{t_i})\|_2^2 \right] \quad (62)$$

$$\text{s.t. } \mathbf{x}_{t_j}^{\text{ODE}} = \mathbf{x}_{t_i} + \int_{t_i}^{t_j} \mathcal{P}(\mathbf{x}_t^{\text{ODE}}) - \frac{1}{2}g^2(t)s_\theta(\mathbf{x}_t^{\text{ODE,F}}, t)dt. \quad (63)$$

By additionally including the time backwards direction where  $t_i > t_j$ , we get the multi step formulation from equation (10), i.e.

$$\mathcal{L}_{\text{multi}}(\theta) = \mathbb{E}_{(\mathbf{x}_{t_i}, \dots, \mathbf{x}_{t_j})} \left[ \sum_{k=i+1}^{j-1} \|\mathbf{x}_{t_k} - \mathbf{x}_{t_k}^{\text{ODE,F}}(\mathbf{x}_{t_i})\|_2^2 + \|\mathbf{x}_{t_k} - \mathbf{x}_{t_k}^{\text{ODE,B}}(\mathbf{x}_{t_j})\|_2^2 \right] \quad (64)$$

$$\text{s.t. } \mathbf{x}_{t_j}^{\text{ODE,F}} = \mathbf{x}_{t_i} + \int_{t_i}^{t_j} \mathcal{P}(\mathbf{x}_t^{\text{ODE,F}}) - \frac{1}{2}g^2(t)s_\theta(\mathbf{x}_t^{\text{ODE,F}}, t)dt, \quad (65)$$

$$\text{and } \mathbf{x}_{t_i}^{\text{ODE,B}} = \mathbf{x}_{t_j} + \int_{t_j}^{t_i} \mathcal{P}(\mathbf{x}_t^{\text{ODE,B}}) - \frac{1}{2}g^2(t)s_\theta(\mathbf{x}_t^{\text{ODE,B}}, t)dt. \quad (66)$$

#### A.4 IMPLEMENTATION

In this section, we give additional details on estimating the loss, how we implement the ODE solver and the sliding window method.

**Estimating the loss** The training data set  $\{(\mathbf{x}_{t_i, n})_{i=0, \dots, M}\}_{n=0, \dots, N}$  is sampled directly from the SDE of the physical system equation (14), so the empirical distribution  $p_{t_i}^{\text{emp}}$  induced by the training data set at time discretization  $t_i$  is close to the marginal distribution  $p_{t_i}$  for  $0 \leq i \leq M$  and sufficiently large  $N$ . We make use of this fact to approximate the sampling of  $\mathbf{x}_{t_i} \sim p_{t_i}$  and  $\mathbf{x}_{t_{i+1}} \sim p_{t_{i+1}}|\mathbf{x}_{t_i}$ , by drawing a data sample  $\mathbf{x}_{t_i}$  at time  $t_i$  and its next successor  $\mathbf{x}_{t_{i+1}}$  on the trajectory at time  $t_{i+1}$  from the training data set.

**ODE solver** In the training, we use Euler steps for the time integration to implement the ODE solver. This is required to estimate the loss  $\mathcal{L}_{\text{multi}}(\theta)$  for the multi step formulation (and single step formulation as a special case). Here, we only consider the time forward direction. The time backward direction is analogous. In this case, the (forward only) multi step loss is given by

$$\mathbb{E}_{(\mathbf{x}_{t_i}, \dots, \mathbf{x}_{t_j})} \left[ \sum_{k=i+1}^{j-1} \|\mathbf{x}_{t_k} - \mathbf{x}_{t_k}^{\text{ODE}}(\mathbf{x}_{t_i})\|_2^2 \right] \quad (67)$$

$$\text{s.t. } \mathbf{x}_{t_j}^{\text{ODE}} = \mathbf{x}_{t_i} + \int_{t_i}^{t_j} \mathcal{P}(\mathbf{x}_t^{\text{ODE}}) - \frac{1}{2}g^2(t)s_\theta(\mathbf{x}_t^{\text{ODE,F}}, t)dt. \quad (68)$$

Using Euler steps for the ODE solver, we can instead optimize

$$\sum_{k=i+1}^{j-1} \|\mathbf{x}_{t_k} - \mu_{\text{ODE}}^k(\mathbf{x}_{t_i})\|_2^2, \quad (69)$$

where  $\mu_{\text{ODE}}^k(\mathbf{x}_{t_i})$  is the discretized trajectory, i.e.

$$\mu_{\text{ODE}}^i(\mathbf{x}_{t_i}) = \mathbf{x}_{t_i} \quad (70)$$

$$\mu_{\text{ODE}}^k(\mathbf{x}_{t_i}) = \mu_{\text{ODE}}^{k-1}(\mathbf{x}_{t_i}) + (t_k - t_{k-1}) \left[ \mathcal{P}(\mu_{\text{ODE}}^{k-1}(\mathbf{x}_{t_i})) - \frac{1}{2}g_{t_k}^2 s_\theta(\mu_{\text{ODE}}^{k-1}(\mathbf{x}_{t_i}), t_{k-1}) \right]. \quad (71)$$

Figure 11 gives an overview how gradients can be backpropagated through the solver steps.

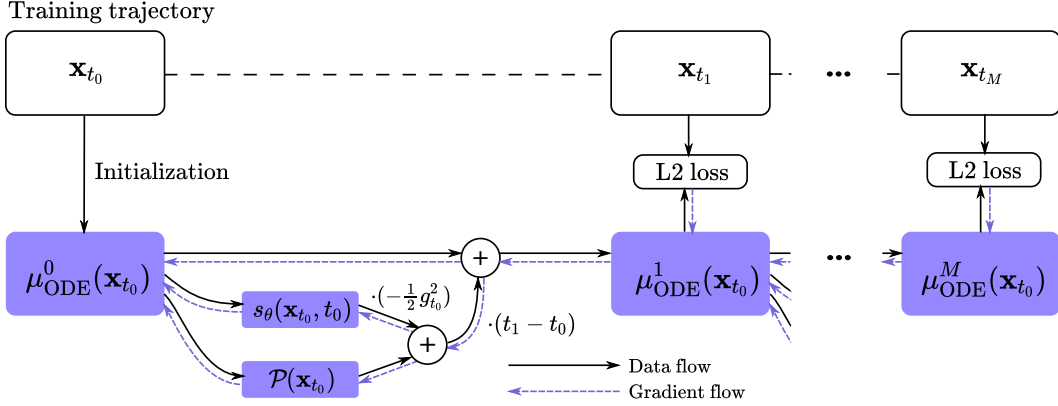


**Figure 11:** Training overview for the trajectory  $(\mathbf{x}_{t_0}, \mathbf{x}_{t_1}, \dots, \mathbf{x}_{t_M})$ . Gradients are backpropagated over multiple time steps via automatic differentiation. This requires that the physics operator  $\mathcal{P}$  is differentiable. Incoming gradients at  $s_\theta(\mathbf{x}_{t_i}, t_i)$  are used to obtain gradients for  $\theta$ , which are summed over all steps  $i$ . The network weights  $\theta$  are then updated based on the optimizer, e.g. stochastic gradient descent or Adam.

**Sliding window and rollout length** For a window size  $S$  and time  $t_i$ , we consider the points  $(\mathbf{x}_{t_i}, \mathbf{x}_{t_{i+1}}, \dots, \mathbf{x}_{t_{i+S}})$  from a sampled training trajectory and compute the probability flow trajectory according to the multi step formulation equation (10). We estimate the loss and backpropagate gradients through all steps to obtain updates for  $\theta$ . Then, we move the window by 1, i.e. consider the points  $(\mathbf{x}_{t_{i+1}}, \mathbf{x}_{t_{i+2}}, \dots, \mathbf{x}_{t_{i+1+S}})$  and compute the updates for  $\theta$ . We repeat the above starting with  $i = 1$  until  $i = M$  to cover the entire simulation trajectory.

For  $S = 2$  we do not require differentiability of the physics operator  $\mathcal{P}$ , as our method reduces to predicting the next point on the trajectory given the previous point, i.e. the single step formulation.

Starting with an untrained score network, long rollouts may yield divergent trajectories because of the physics dynamics. Therefore, losses may be very high and the training becomes unstable. For this reason, we start training with the single step formulation and a sliding window of size 2. We train for a fixed number of epochs and then increase the sliding window size  $S$  by a constant. We repeat this until we reach a sufficiently high rollout length, which yields stable trajectories for the entire simulation.

We give details of the sliding windows size for each specific experiment either directly in the main text or the accompanying appendix.

**Inference** For inference and a given simulation end state  $\mathbf{x}_T$ , we obtain a trajectory by solving the probability flow ODE (SMDP-ODE) or simulating paths from the reverse-time SDE (SMDP-SDE) to obtain samples from the posterior. In both cases, we can plug in the same learned network  $s_\theta(\mathbf{x}, t)$ . We use the explicit Euler method as ODE solver and the Euler-Maruyama method as SDE solver. In all experiments, the time discretization for inference is the same as the one used during training unless stated otherwise. An algorithm for inference for the ODE and SDE variant is given in algorithm 1.

---

**Algorithm 1** SMDP-ODE, SMDP-SDE
 

---

**Require:**  $\mathbf{x}_{t_M}, \{t_m\}_{m=0}^M, \{g_{t_m}\}_{m=0}^M$   
 1: **for**  $m \leftarrow M$  **to** 1 **do**  
 2:    $\mathbf{p} \leftarrow \mathcal{P}(\mathbf{x}_{t_m})$   
 3:    $\mathbf{s} \leftarrow -g_{t_m}^2 s_\theta(\mathbf{x}_{t_m}, t_m)/2$   
 4:   **if** SMDP-ODE **then**  
 5:      $\mathbf{x}_{t_{m-1}} \leftarrow \mathbf{x}_{t_m} - (t_m - t_{m-1}) \cdot (\mathbf{p} + \mathbf{s})$   
 6:   **if** SMDP-SDE **then**  
 7:      $\mathbf{x}_{t_{m-1}} \leftarrow \mathbf{x}_{t_m} - (t_m - t_{m-1}) \cdot (\mathbf{p} + 2\mathbf{s})$   
 8:      $z \sim \mathcal{N}(0, I)$   
 9:      $\mathbf{x}_{t_{m-1}} \leftarrow \mathbf{x}_{t_{m-1}} + g_{t_m} \sqrt{t_m - t_{m-1}} z$   
 10: **return**  $\mathbf{x}_{t_0}$

---

### A.5 BACKWARD ONLY AND SDE TRAINING

We discuss two variants of the SMDP training. First, we consider a formulation based on the probability flow, but which only considers solving the probability flow ODE with a backward time integration, named *backward only probability flow training*. Then, we consider an implementation-wise similar variant, which is based on directly training the reverse-time SDE, named *SDE training*. We show that in both cases the network  $s_\theta(\mathbf{x}, t)$  learns the correct score.

**Backward only probability flow training** In the single step and multi step formulation, we require to solve the probability flow ODE forward and backwards in time, which requires additional computational effort compared to solving for only one time direction. For the single step formulation, we may consider only minimizing the backward direction objective (cf. equation (24))

$$\text{KL}(p_{t_{i-1}} \times p_{t_i} \parallel p_{t_{i-1}}^{t_i, \text{ODE}} \times p_{t_i}). \quad (72)$$

With an analogous derivation as in appendix A.3, we can show that the optimal network weights for  $s_\theta(\mathbf{x}, t)$  minimize

$$\frac{1}{\epsilon^2} \Delta t^2 g(t_i)^4 \mathbb{E}_{\mathbf{x}_{t_i}} [\|\nabla_{\mathbf{x}} \log p_t(\mathbf{x}_{t_i}) - \frac{1}{2} s_\theta(\mathbf{x}_{t_i}, t_i)\|_2^2], \quad (73)$$

which is minimized if  $\frac{1}{2} s_\theta(\mathbf{x}, t) \equiv \nabla_{\mathbf{x}} \log p_t(\mathbf{x})$ . Therefore, using the loss

$$\mathcal{L}_{\text{single, B}}(\theta) = \mathbb{E}_{(\mathbf{x}_{t_i}, \mathbf{x}_{t_{i+1}})} \left[ \|\mathbf{x}_{t_i} - \mu_{t_i}^{t_{i+1}, \text{ODE}}(\mathbf{x}_{t_{i+1}})\|_2^2 \right], \quad (74)$$

the score network  $s_\theta(\mathbf{x}, t)$  learns to approximate  $2\nabla_{\mathbf{x}} \log p_t(\mathbf{x})$ , which is proportional to the correct score.

We can correct for the factor 2 during training by directly modifying the probability flow ODE to a new ODE such that  $s_\theta(\mathbf{x}, t)$  learns the exact score.

In particular, this means changing the probability flow ODE from

$$d\mathbf{x} = [\mathcal{P}(\mathbf{x}) - \frac{1}{2} g^2(t) s_\theta(\mathbf{x}, t)] dt \quad (75)$$

to

$$d\mathbf{x} = [\mathcal{P}(\mathbf{x}) - g^2(t) s_\theta(\mathbf{x}, t)] dt \quad (76)$$

and modifying the approximations in equation (32) and equation (33) accordingly. Moreover, this updates the multi step loss  $\mathcal{L}_{\text{multi}}(\theta)$  to

$$\mathcal{L}_{\text{multi, B}}(\theta) = \mathbb{E}_{(\mathbf{x}_{t_i}, \dots, \mathbf{x}_{t_j})} \left[ \sum_{k=i+1}^{j-1} \|\mathbf{x}_{t_k} - \mathbf{x}_{t_k}^{\text{ODE, B}}(\mathbf{x}_{t_j})\|_2^2 \right] \quad (77)$$

$$\text{s.t. } \mathbf{x}_{t_i}^{\text{ODE, B}} = \mathbf{x}_{t_j} + \int_{t_j}^{t_i} \mathcal{P}(\mathbf{x}_t^{\text{ODE, B}}) - g^2(t) s_\theta(\mathbf{x}_t^{\text{ODE, B}}, t) dt. \quad (78)$$



**SDE Training** Instead of considering the probability flow ODE and induced probabilities  $p_{t_{i-1}}^{t_i, \text{ODE}}$  in the single step formulation, we can also directly optimize the SDE, i.e.

$$\text{KL}(p_{t_{i-1}} \times p_{t_i} \| p_{t_{i-1}}^{t_i, \text{SDE}} \times p_{t_i}), \quad (79)$$

where  $p_{t_{i-1}}^{t_i, \text{SDE}}$  is defined by sampling  $\mathbf{x} \sim p_{t_i}$  and solving the reverse-time SDE until time  $t_{i-1}$ . Note that unlike for the probability flow ODE, we cannot include the forward time direction in the objective, as the evolution of marginal likelihoods for the reverse-time SDE is only correct in the backward time direction and is not bidirectional. We can analogously follow the derivation of the single step formulation for the probability flow ODE, but now model the conditional distribution  $p_{t_{i-1}}^{t_i, \text{SDE}} | \mathbf{x}_{t_i}$  as a Gaussian distribution with mean

$$\mu_{t_{i-1}}^{t_i, \text{SDE}}(\mathbf{x}_{t_i}) = \mathbf{x}_{t_i} - \Delta t [\mathcal{P}(\mathbf{x}_{t_i}) - g(t_i)^2 s_\theta(\mathbf{x}_{t_i}, t_i)] \quad (80)$$

and standard deviation  $\sigma = \sqrt{\Delta t} g(t_{i+1})$  (instead of the perturbed ODE distribution). Then, the single step SDE loss becomes

$$\mathcal{L}_{\text{single, SDE}}(\theta) = \mathbb{E}_{(\mathbf{x}_{t_i}, \mathbf{x}_{t_{i+1}})} [\|\mathbf{x}_{t_i} - \mu_{t_i}^{\text{SDE}}(\mathbf{x}_{t_{i+1}})\|_2^2], \quad (81)$$

and the multi step loss

$$\mathcal{L}_{\text{multi, SDE}}(\theta) = \mathbb{E}_{(\mathbf{x}_{t_i}, \dots, \mathbf{x}_{t_j})} \left[ \sum_{k=i+1}^{j-1} \|\mathbf{x}_{t_k} - \mathbf{x}_{t_k}^{\text{SDE}}(\mathbf{x}_{t_j})\|_2^2 \right] \quad (82)$$

$$\text{s.t. } \mathbf{x}_{t_i}^{\text{SDE}} = \mathbf{x}_{t_j} + \int_{t_j}^{t_i} \mathcal{P}(\mathbf{x}_t^{\text{SDE}}) - g^2(t) s_\theta(\mathbf{x}_t^{\text{SDE, B}}, t) dt + \int_{t_j}^{t_i} g(t) dw. \quad (83)$$

#### A.6 SEPARATING PHYSICS AND SCORE UPDATES FOR DETERMINISTIC SYSTEMS

When separating physics and score update, cf. figure 3c, for the single step formulation from  $t_{i+1}$  to  $t_i$ , we effectively train a denoising network  $s_\theta(\mathbf{x}, t)$  for each time step  $t$  and calculate the updates as

$$\hat{\mathbf{x}}_{t_i} = \mathbf{x}_{t_{i+1}} - \Delta t \mathcal{P}(\mathbf{x}_{t_{i+1}}) \quad (84)$$

$$\hat{\mathbf{x}}_{t_i}^{\text{noise}} = \hat{\mathbf{x}}_{t_i} + \sqrt{\Delta t} g(t_i) z_{t_i} \quad (85)$$

$$\mathbf{x}_{t_i} = \hat{\mathbf{x}}_{t_i}^{\text{noise}} + \Delta t g^2(t_i) s_\theta(\hat{\mathbf{x}}_{t_i}^{\text{noise}}, t_i), \quad (86)$$

where  $z_{t_i} \sim \mathcal{N}(0, I)$ . If the physical system is deterministic and  $\Delta t$  is small enough, then we can approximate  $\mathbf{x}_{t_i} \approx \hat{\mathbf{x}}_{t_i}$  and for the moment, we assume that we can write

$$\hat{\mathbf{x}}_{t_i}^{\text{noise}} = \mathbf{x}_{t_i} + \sqrt{\Delta t} g(t_i) z_{t_i}. \quad (87)$$

In this case, we can rewrite the single step loss  $\mathcal{L}_{\text{single}}(\theta)$  from equation (9) to obtain the denoising score matching loss

$$\mathcal{L}_{\text{DSM}}(\theta) := \mathbb{E}_{(\mathbf{x}_{t_i}, \mathbf{x}_{t_{i+1}})} [\|\mathbf{x}_{t_i} - \hat{\mathbf{x}}_{t_i}^{\text{noise}} - \Delta t g^2(t_i) s_\theta(\hat{\mathbf{x}}_{t_i}^{\text{noise}}, t_i)\|_2^2], \quad (88)$$

which is the same as minimizing

$$\mathbb{E}_{(\mathbf{x}_{t_i}, \mathbf{x}_{t_{i+1}})} \left[ \left\| s_\theta(\tilde{\mathbf{x}}_{t_i}^{\text{noise}}, t_i) - \frac{1}{\Delta t g^2(t_i)} (\mathbf{x}_{t_i} - \tilde{\mathbf{x}}_{t_i}^{\text{noise}}) \right\|_2^2 \right]. \quad (89)$$

Now, the idea presented in Vincent (2011) is that for score matching, we can consider a joint distribution  $p_{t_i}(\mathbf{x}_{t_i}, \tilde{\mathbf{x}}_{t_i})$  of sample  $\mathbf{x}_{t_i}$  and corrupted sample  $\tilde{\mathbf{x}}_{t_i}$ . Using Bayes' rule, we can write  $p_{t_i}(\mathbf{x}_{t_i}, \tilde{\mathbf{x}}_{t_i}) = p_\sigma(\tilde{\mathbf{x}}_{t_i} | \mathbf{x}_{t_i}) p_{t_i}(\mathbf{x}_{t_i})$ . The conditional distribution  $p_\sigma(\cdot | \mathbf{x}_{t_i})$  for the corrupted sample is then modeled by a Gaussian with standard deviation  $\sigma = \sqrt{\Delta t} g(t_i)$ , i.e. we can write  $\tilde{\mathbf{x}} = \mathbf{x} + \sqrt{\Delta t} g(t_i) z$  for  $z \sim \mathcal{N}(0, I)$  similar to equation equation (87). Moreover, we can define the distribution of corrupted data  $q_\sigma$  as

$$q_\sigma(\tilde{\mathbf{x}}) = \int p_\sigma(\tilde{\mathbf{x}} | \mathbf{x}) p_{t_i}(\mathbf{x}) d\mathbf{x}. \quad (90)$$

If  $\sigma$  is small, then  $q_\sigma \approx p_{t_i}$  and  $\text{KL}(q_\sigma \| p_{t_i}) \rightarrow 0$  as  $\sigma \rightarrow 0$ . Importantly, in this case we can directly compute the score for  $p_\sigma(\cdot | \mathbf{x})$  as

$$\nabla_{\tilde{\mathbf{x}}} \log p_\sigma(\tilde{\mathbf{x}} | \mathbf{x}) = \frac{1}{\sigma^2}(\mathbf{x} - \tilde{\mathbf{x}}). \quad (91)$$

Moreover, the theorem by Vincent (2011) means that we can use the score of the conditional distribution  $p_\sigma(\cdot | \mathbf{x})$  to train  $s_\theta(\mathbf{x}, t)$  to learn the score of  $q_\sigma(\mathbf{x})$ , i.e.

$$\arg \min_{\theta} \mathbb{E}_{\tilde{\mathbf{x}} \sim q_\theta} [\|s_\theta(\mathbf{x}, t_i) - \nabla_{\tilde{\mathbf{x}}} \log q_\sigma(\tilde{\mathbf{x}})\|_2^2] \quad (92)$$

$$= \arg \min_{\theta} \mathbb{E}_{\mathbf{x} \sim p_{t_i}, \tilde{\mathbf{x}} \sim p_\sigma(\cdot | \mathbf{x})} [\|s_\theta(\mathbf{x}, t_i) - \nabla_{\tilde{\mathbf{x}}} \log p_\sigma(\tilde{\mathbf{x}} | \mathbf{x})\|_2^2]. \quad (93)$$

By combining equation (93) and equation (91), this exactly equals the denoising loss  $\mathcal{L}_{\text{DSM}}(\theta)$  in equation (89). As  $q_\sigma \approx p_{t_i}$ , we also obtain that  $\nabla_{\mathbf{x}} \log q_\sigma(\mathbf{x}) \approx \nabla_{\mathbf{x}} \log p_{t_i}(\mathbf{x})$ , so the network  $s_\theta(\mathbf{x}, t_i)$  approximately learns the correct score for  $p_{t_i}$ .

We have made the assumption in equation (87) that the only corruption for  $\hat{\mathbf{x}}_{t_i}^{\text{noise}}$  is the Gaussian noise. This is not true, as in fact we have

$$\hat{\mathbf{x}}_{t_i}^{\text{noise}} = \mathbf{x}_{t_i} + \sqrt{\Delta t} g(t_i) z_{t_i} + (\mathbf{x}_{t_{i+1}} - \Delta t \mathcal{P}(\mathbf{x}_{t_{i+1}}) - \mathbf{x}_{t_i}), \quad (94)$$

so there is an additional source of corruption, which comes from the numerical errors due to the term  $\mathbf{x}_{t_{i+1}} - \Delta t \mathcal{P}(\mathbf{x}_{t_{i+1}}) - \mathbf{x}_{t_i}$ . This means that the conditional distribution  $p_\sigma(\cdot | \mathbf{x})$  is only approximately a Gaussian. Ideally, the effects of numerical errors are dominated by the Gaussian random noise. However, for a longer sequence of inference steps, even small errors may accumulate. To account for this, we argue that the multi step loss  $\mathcal{L}_{\text{multi}}(\theta)$  should be considered analogously to the SDE case as discussed in section 3. During training, with the separation of physics update and denoising the simulation state is first progressed from time  $t_{i+1}$  to time  $t_i$  using the physics solver. This only yields a perturbed version of the simulation at time  $t_i$  due to numerical inaccuracies. Then a small Gaussian noise is added and via the denoising network  $s_\theta(\mathbf{x}, t)$ , the simulation state is projected back to the distribution  $p_{t_i}$ , which should also resolve the numerical errors. This is iterated as discussed in section 3 depending on the sliding window size and location.

## B ADDITIONAL EXPERIMENT: 1D PROCESS

We discuss an additional experiment, where we compare SMDP with Implicit Score Matching (ISM) (Hyvärinen, 2005). For this task, we consider the SDE given by

$$dx = - [\lambda_1 \cdot \text{sign}(x)x^2] dt + \lambda_2 dw, \quad (95)$$

with  $\lambda_1 = 7$  and  $\lambda_2 = 0.03$ . The corresponding reverse-time SDE is given by

$$dx = - [\lambda_1 \cdot \text{sign}(x)x^2 - \lambda_2^2 \cdot \nabla_x \log p_t(x)] dt + \lambda_2 dw. \quad (96)$$

Throughout this experiment,  $p_0$  is a categorical distribution, where we draw either 1 or  $-1$  with the same probability. In figure 12, we show trajectories from this SDE simulated with the Euler-Maruyama method. Trajectories either start at 1 or  $-1$  and approach 0 as  $t$  increases. Given the trajectory value at  $t = 10$ , it is no longer possible to infer the origin of the trajectory at  $t = 0$ .

We employ a neural network  $s_\theta(x, t)$  parameterized by  $\theta$  to approximate the score via ISM and compare it to SMDP. In both cases, the neural network is a simple multilayer perceptron with elu activations and 5 hidden layers with 30, 30, 25, 20 and then 10 neurons for the last hidden layer.

Our training data set consists of 250 simulated trajectories from  $t = 0$  until  $t = 10$  and  $\Delta t = 0.02$ . Therefore each training trajectory has length  $M = 500$ .

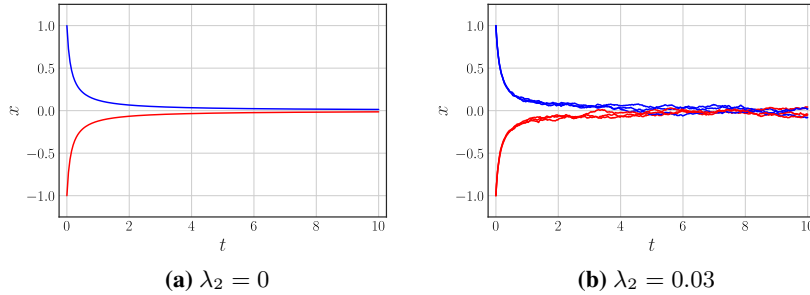


**Figure 12:** Trajectories from SDE equation (95) with  $\lambda_2 = 0$  (a) and  $\lambda_2 = 0.03$  (b).

**Implicit Score Matching** Implicit Score Matching (Hyvärinen, 2005) is a score matching method that leverages the fact that for a random vector  $\mathbf{x} \in \mathbb{R}^d$  with probability density function  $p$ , minimizing the score matching objective

$$J(\theta) := \frac{1}{2} \mathbb{E}_{\mathbf{x} \sim p} [\|s_\theta(\mathbf{x}) - \nabla_{\mathbf{x}} \log p(\mathbf{x})\|_2^2] \quad (97)$$

is equivalent to minimizing the following objective

$$J'(\theta) := \mathbb{E}_{\mathbf{x} \sim p} \left[ \sum_{i=1}^d \frac{\partial s_\theta(\mathbf{x})_i}{\partial \mathbf{x}_i} + \frac{1}{2} s_\theta(\mathbf{x})_i^2 \right]. \quad (98)$$

Note that for ISM, there is no explicit time dimension, so we are absorbing the time dimension into  $\mathbf{x}$ , i.e. for the trajectory  $(x_1, x_2, \dots, x_M)$  sampled at time  $(t_1, t_2, \dots, t_M)$ , we concatenate value and time with  $\mathbf{x}^{(i)} := (x_i, t_i) \in \mathbb{R}^2$ . We collect  $\mathbf{x}_i$  for  $i = 1, \dots, M$  from all trajectories in a new training data set. When training  $s_\theta(\mathbf{x})$ , we therefore lose the information, to which trajectory a value-time pair originally belonged. We obtain the time-dependent score  $\nabla_{\mathbf{x}_1} \log p_{\mathbf{x}_2}(\mathbf{x}_1)$  from the first coordinate of the output of  $s_\theta(\mathbf{x})$ , i.e.  $s_\theta(\mathbf{x})_1$ .

We compute the partial derivative  $\partial s_\theta(\mathbf{x})_i / \partial \mathbf{x}_i$  using reverse-mode automatic differentiation in JAX (jax.jacrev). We train  $s_\theta(\mathbf{x})$  with a batch size of 10,000 and the Adam optimizer for 15,000 epochs with learning rate  $5.0e^{-4}$ , which we decrease by a factor of 0.1 every 50,000 batches. With this setup, we found that the learned score is inaccurate, e.g. it is not symmetric around the  $x$ -axis, cf. figure 13a. We therefore include an additional loss term  $\|s_\theta((\mathbf{x}, t)) + s_\theta((-\mathbf{x}, t))\|_2^2$  during training, which enforces the symmetry.

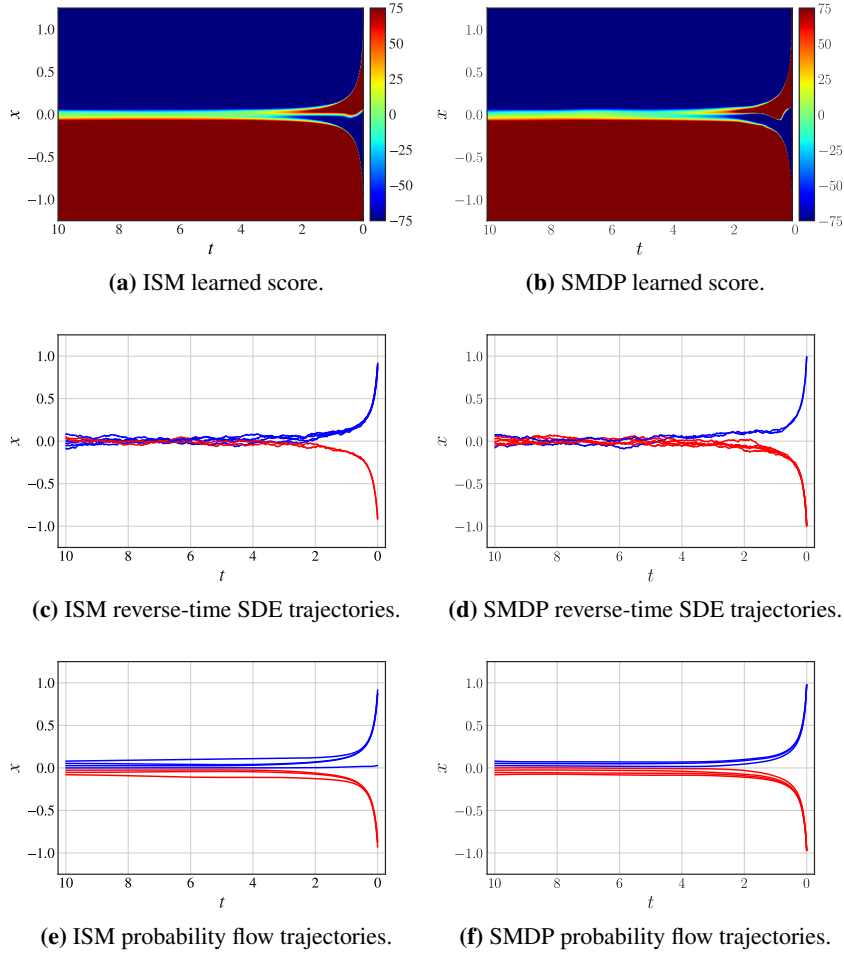


**Figure 13:** Comparison of Implicit Score Matching (ISM, left) and Score Matching via Differentiable Physics (SMDP, right). Colormap in (a) and (b) truncated to  $[-75, 75]$ .

**SMDP Training** First, we train the network  $s_\theta(\mathbf{x}, t)$  for 2,500 epochs with the single step formulation (sliding window  $S = 2$ ), batch size 256, learning rate  $1.0 \times 10^{-3}$  and Adam optimizer. Then we finetune the network with learning rate  $1.0 \times 10^{-4}$  for an additional 500 steps. For this toy experiment, we found that the single step formulation is already sufficient to yield stable trajectories and a good score approximation. We do not require an additional symmetry loss term in this case.

**Comparison** We show a direct comparison of the learned score, the reverse-time SDE trajectories and the probability flow trajectories between ISM and SMDP in figure 13. The learned score of ISM and SMDP in figure 13a and figure 13b is very similar, showing that our method and loss learns the correct score. Overall, after finetuning both ISM and SMDP, the SMDP trajectories are slightly more accurate. For example, in figure 13e there is a trajectory that ends in 0 instead of  $-1$  or  $1$ . Also, for both ODE and SDE trajectories, SMDP trajectories end in either  $-1$  or  $1$ , but ISM trajectories stop shortly before reaching either  $-1$  or  $1$ .

Overall, this example illustrates that the learned score of SMDP is slightly more accurate than the one of ISM. For ISM, we also only show results where we included the additional symmetry loss in the training and which gave considerable improvements.

## C 1D HEAT EQUATION: EVALUATION OF POSTERIOR

To demonstrate the diversity and high quality of the reverse-time SDE trajectories we provide an additional evaluation of the posterior for the one-dimensional heat equation case. We compare the SDE solutions with samples obtained from filtering a large data set. To simplify the comparison, we consider 1D processes based on the 2D Gaussian random fields from section 4.1. Each process has a length of 100 and corresponds to a Gaussian random field of size  $1 \times 100$ . Analogously to section 4.1, we use the heat equation to simulate the states forward in time from  $t = 0.0$  until  $t = 0.2$ . Figure 14 shows some examples of the 1D processes we consider here.

**Training of SMDP** The network  $s_\theta(\mathbf{x}, t)$  representing the score is trained as described for the heat equation experiment, section 4.1, using the same ResNet architecture with padding in  $y$ -direction removed. We consider a time discretization with  $\Delta t = 0.01$ . We begin training with an initial rollout of 6 steps and increase the rollout length every 5 epochs by 2 until we reach 14 rollout steps. For every epoch, we train on 20 randomly generated 1D processes. We use the Adam optimizer with learning rate  $10^{-4}$ .

In the following, we randomly generate a 1D process  $P$  and describe how we generate samples for  $t = 0.0$  conditioned on the simulation end state of  $P$  at  $t = 0.2$ .

**Reverse-SDE posterior** We initialize the state based on  $P$  at  $t = 0.2$ . Then, we simulate the reverse-time SDE with the learned score  $s_\theta(\mathbf{x}, t)$  via Euler-Maruyama steps. A visualization of 100 samples is shown in figure 16.

**Empirical distribution** We sample  $10^6$  processes and form pairs of initial state  $t = 0$  and end states  $t = 0.2$ . We filter the 100 process end states that are closest to the end state of  $P$  in terms of the L2 distance. As solutions from the empirical sampling, we consider the 100 corresponding initial states as shown in figure 15.

This empirical distribution makes a qualitative comparison possible, as shown in figures 16 and 15. This illustrates that the reverse-time SDE solutions are diverse while matching  $P$  very well at. Simulating the obtained solutions forward in time gives end state at  $t = 0.2$  that are in excellent agreement with  $P$ .

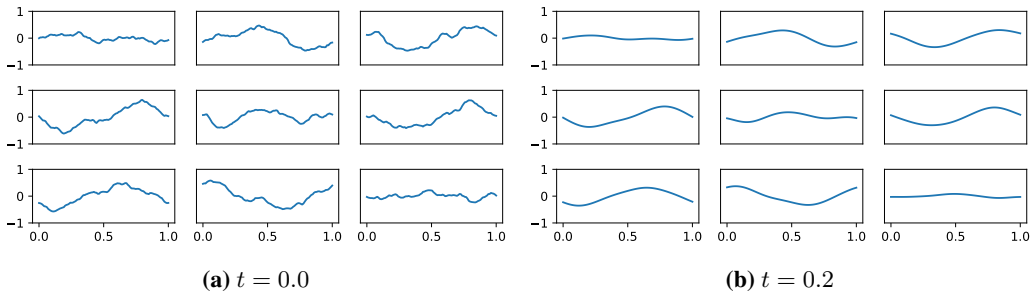


**Figure 14:** Examples of training data for 1D heat equation with initial states at  $t = 0.0$  (a) and end states at  $t = 0.2$  (b).

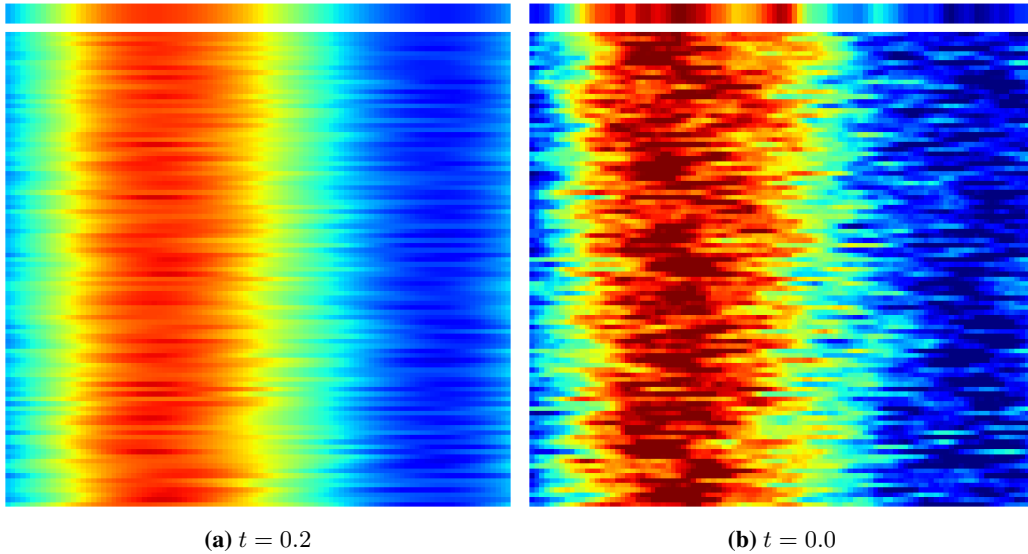


**Figure 15: Empirical distribution:** we generate  $10^6$  Gaussian processes and simulate them forward in time from  $t = 0.0$  until  $t = 0.2$ . We pick one specific process  $P$  and sort all other processes in ascending order based on the  $L_2$  distance to  $P$  at time  $t = 0.2$ . Then, we select the first 100 processes and visualize them at time  $t = 0.0$  (a) and  $t = 0.2$  (b). The top row in both plots shows the process  $P$ .

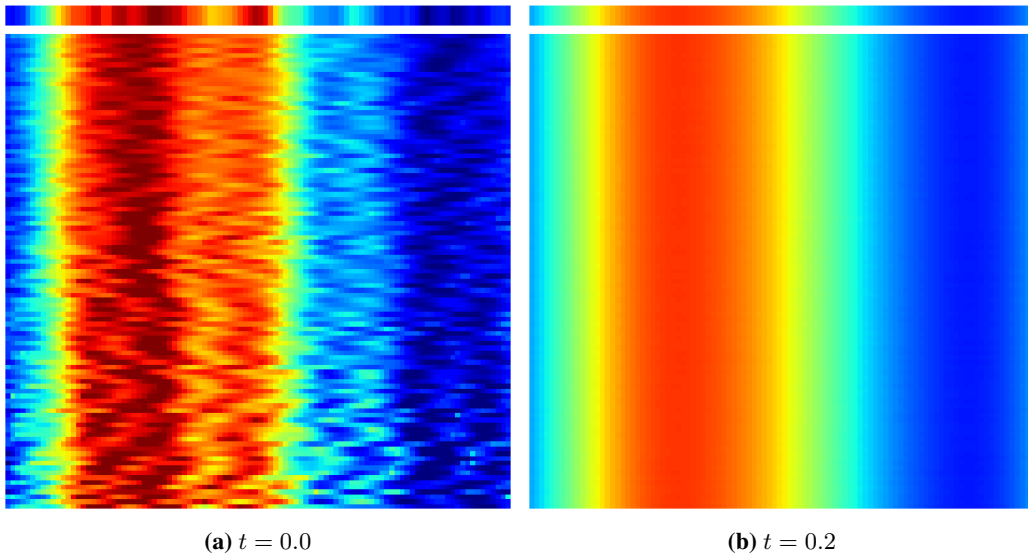


**Figure 16: Reverse-time SDE:** We pick the process  $P$  from figure 15. Then, we simulate 100 trajectories from the reverse-time SDE with learned score and  $P$  at  $t = 0.2$  as initialization. We sort the states at  $t = 0.0$  based on their  $L_2$  distance to  $P$  and visualize them (a). We then simulate all states from (a) forward in time until  $t = 0.2$ , see (b). The forward simulated trajectories almost exactly match  $P$  at  $t = 0.2$ .

---

## D ARCHITECTURES

**ResNet** We employ a simple ResNet-like architecture, which is used in Section 4.1 for the score function  $s_\theta(\mathbf{x}, t)$  and the convolutional neural network baseline (ResNet-S and ResNet-P) as well as in Section 4.3 again for the score  $s_\theta(\mathbf{x}, t)$ .

For experiments with periodic boundary conditions, we apply a periodic padding with length 16, i.e. if the underlying 2-dimensional data dimensions are  $N \times N$ , the dimensions after the periodic padding are  $(N + 16) \times (N + 16)$ . We implement the periodic padding by first tiling the input 3 times in  $x$ - and  $y$ -direction and then cropping to the correct sizes. The time  $t$  is concatenated as an additional constant channel to the 2-dimensional input data when this architecture is used to represent the score  $s_\theta(\mathbf{x}, t)$ .

The encoder-part of our network begins with a single 2D-convolution encoding layer with 32 filters, kernel size 4 and no activation function. This is followed by 4 consecutive residual blocks, each consisting of 2D-convolution, LeakyReLU, 2D-convolution and Leaky ReLU. All 2D convolutions have 32 filters with kernel size 4 and stride 1. The encoder part ends with a single 2D convolution with 1 filter, kernel size 1 and no activation. Then, in the decoder part, we begin with a transposed 2D convolution, 32 filters, kernel size 4. Afterwards, there are 4 consecutive residual blocks, analogous to the encoder residual blocks, but with the 2D convolution replaced by a transposed 2D convolution. Finally there is a final 2D convolution with 1 filter and kernel size 5. Parameter counts of this model, as well as for other models are given in table 3.

**UNet** We use the UNet architecture with spatial dropout as described in (Mueller et al., 2022), Appendix A.1. The dropout rate is set to 0.25. We do not include batch normalization and apply the same periodic padding as done for our ResNet architecture.

**FNO** For all experiments, we consider the FNO-2D architecture introduced in (Li et al., 2020) with  $k_{\max,j} = 12$  Fourier modes per channel.

**Dil-ResNet** The Dil-ResNet architecture is described in (Stachenfeld et al., 2021), Appendix A. Since this architecture represents the score  $s_\theta(\mathbf{x}, t)$  in Section 4.2, we concatenate the constant time channel analogously to the ResNet architecture. Additionally, positional information is added to the network input by encoding the  $x$ -position and  $y$ -position inside the domain in two separate channels.

Architecture	Parameters
ResNet	330.754
UNet	706.035
DilatedConv	336.915
FNO	465.377

**Table 3:** Summary of architectures.

---

## E HEAT EQUATION

**Spectral solver** The physics of the 2-dimensional heat equation for  $\mathbf{x} \in \mathbb{R}^{d \times d}$  can be computed analytically. The solver  $\mathcal{S}(\mathbf{x}, \Delta t)$  simulates the systems  $\mathbf{x}$  forward in time by  $\Delta t$  using the (shifted) Fourier transformation  $\mathcal{F}$ . In particular, we can implement the solver with

$$\mathcal{S}(\mathbf{x}, \Delta t) = \mathcal{F}^{-1}(A(\Delta t) \circ \mathcal{F}(\mathbf{x})), \quad (99)$$

where  $\circ$  denotes element-wise multiplication and  $A(\Delta t)_{ij} \in \mathbb{R}^{d \times d}$  is a matrix with entries  $A(\Delta t)_{ij} := \exp(-\Delta t \cdot \min(i, j, d - i, j - i))$ . The power spectrum of  $\mathbf{x}$  is scaled down by  $A(\Delta t)$  and higher frequencies are suppressed more than lower frequencies (for  $\Delta t > 0$ ). If noise is added to  $\mathbf{x}$ , then this means that especially higher frequencies are affected. Therefore the inverse transformation (when  $\Delta t > 0$ ) exponentially scales contributions by the noise, causing significant distortions for the reconstruction of  $\mathbf{x}$ .

**Spectral loss** We consider a spectral error based on the two-dimensional power spectral density. For two 2D-images, we compute the 2D Fourier transform and the radially averaged power spectra  $s_1$  and  $s_2$ . Then, we define the spectral error as the weighted difference between the log of the spectral densities

$$\mathcal{L}(s_1, s_2) = \sum_k w_k |\log(s_{1,k}) - \log(s_{2,k})| \quad (100)$$

with a weighting vector  $w \in \mathbb{R}^d$  and  $w_k = 1$  for  $k \leq 10$  and  $w_k = 0$  otherwise.

**Training of  $s_\theta(\mathbf{x}, t)$**  For inference, we consider the linear time discretization  $t_n = n\Delta t$  with  $\Delta t = 0.2/32$  and  $t_{32} = 0.2$ . During training, in order to mitigate the effects of overfitting to  $\Delta t$ , we sample a random time discretization  $\tilde{t}_n$  for each batch based on  $t_n$  by  $\tilde{t}_n \sim \mathcal{U}(t_n - \Delta t/2, t_n + \Delta t/2)$  for  $n = 1, \dots, 31$ . In the warmup phase of training, we consider the multi step loss with a sliding window size of  $S = 6, 8, \dots, 32$  steps, where we increase  $S$  every 2 epochs. We employ Adam to update the weights  $\theta$  with learning rate  $10^{-4}$ . After the warmup is finished, we finetune the network weights for 80 epochs with an initial learning rate of  $10^{-4}$  which we reduce by a factor of 0.5 every 20 epochs.

**HeatGen** The generative model HeatGen is inspired by Rissanen et al. (2022), which propose a classical diffusion-like model that generates data from the dynamics of the heat equation. Nonetheless, the implementation details and methodology is analogous to SMDP, except that the physics operator  $\mathcal{P}$  is not explicitly defined, but instead learned by the network  $s_\theta(\mathbf{x}, t)$  together with the score at the same time. We make use of the same ResNet architecture as SMDP. Except for the physics operator  $\mathcal{P}$ , the training setup is identical to SMDP. During inference, although the network  $s_\theta(\mathbf{x}, t)$  is not trained with any noise for a larger sliding window in the multi step formulation, we may add noise to the simulation states. We add the same noise as for the SMDP-SDE inference in this case. We denote this non-deterministic variant by HeatGen+noise.

**Baseline methods** All other baseline methods are trained for 80 epochs using the Adam optimizer algorithm with an initial learning rate of  $10^{-4}$  which is decreased by a factor of 0.5 every 20 epochs. For the training data, we consider solutions to the heat equation consisting of initial state  $\mathbf{x}_0$  and end state  $\mathbf{x}_T$  created from the heat equation without any non-deterministic dynamics and add a Gaussian noise with standard deviation  $\sigma = 0.1$  to the network input.

### E.1 ADDITIONAL RESULTS

We show visualizations for the predictions of different methods in figure 17 and figure 18.



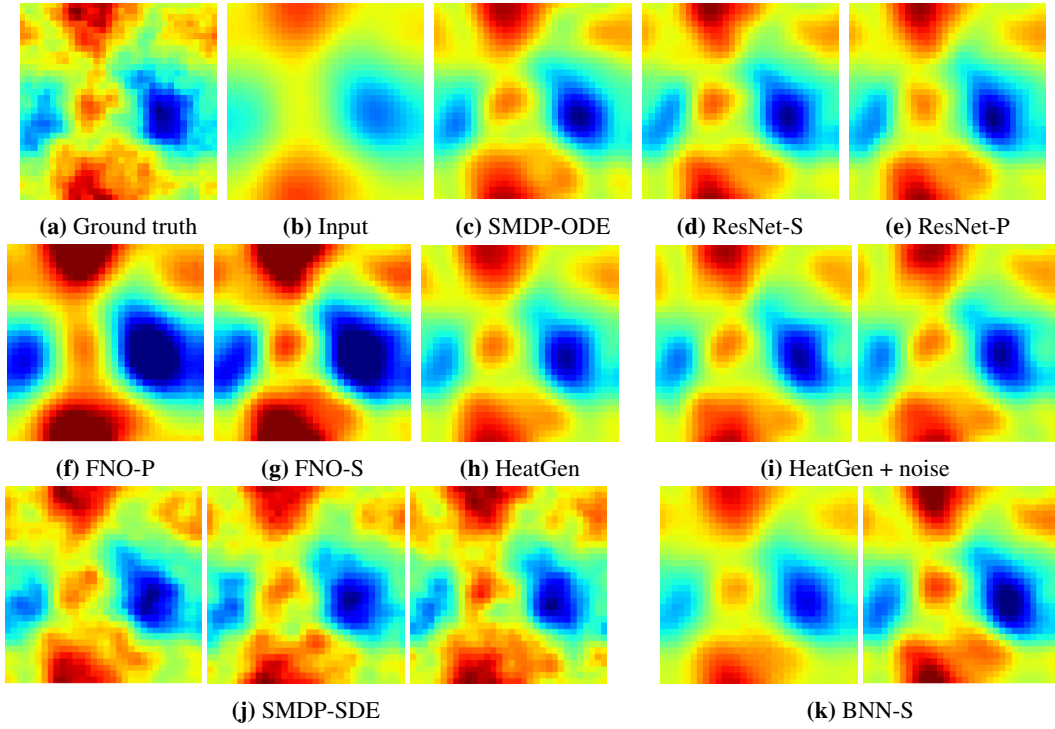


**Figure 17:** Predictions of different methods for the heat equation problem (example 1 of 2).

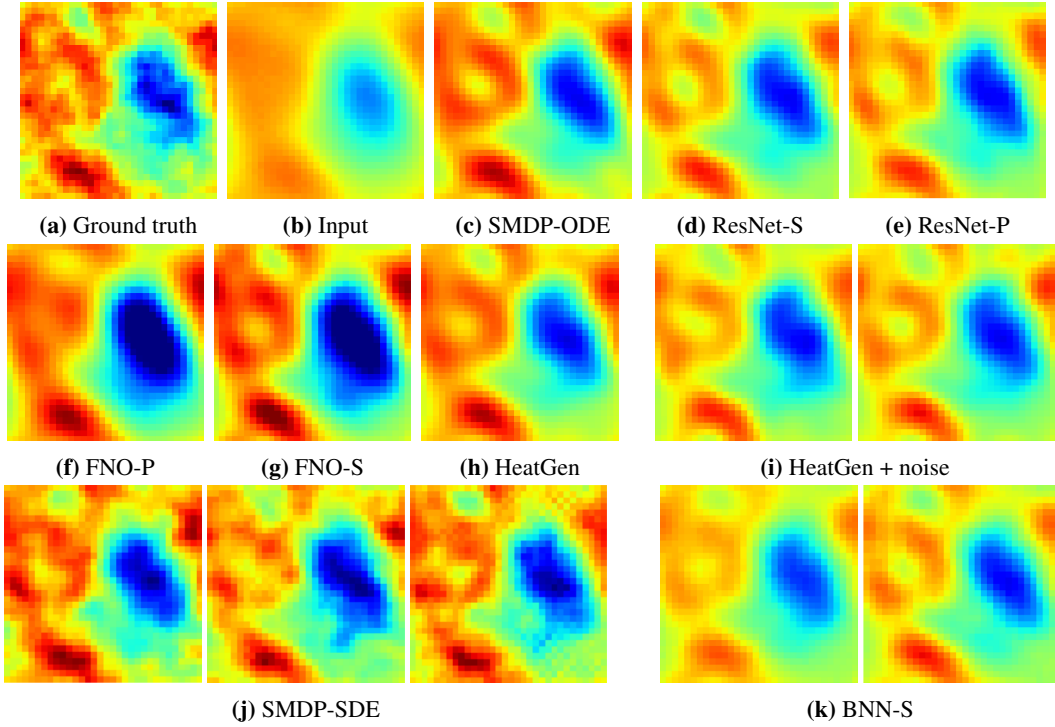


**Figure 18:** Predictions of different methods for the heat equation problem (example 2 of 2). Neither the BNN nor the HeatGen+noise model are able to produce small-scale structures.

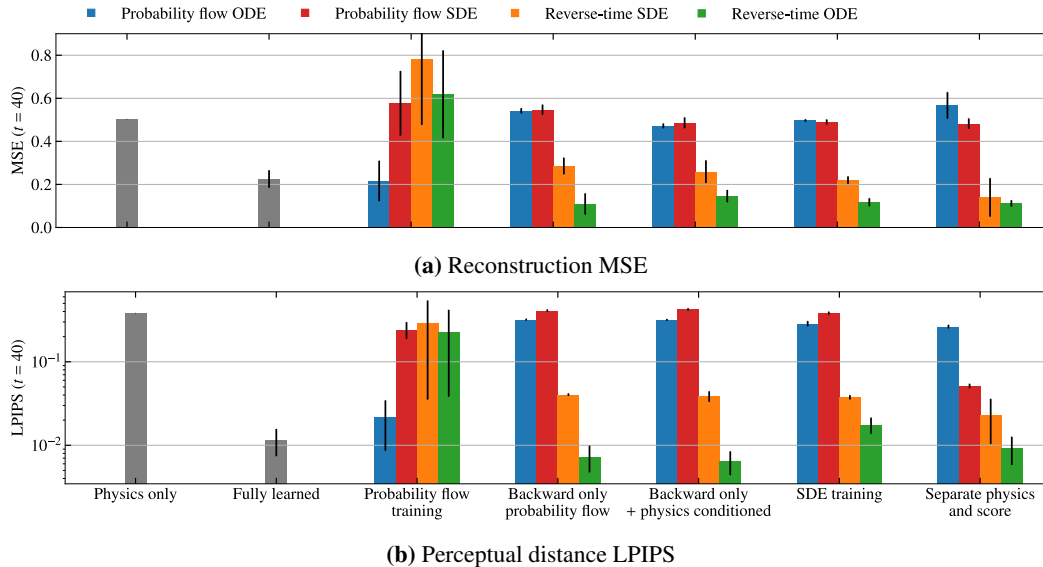


**Figure 19:** Evaluation of training and inference methods for the buoyancy obstacle case in terms of reconstruction MSE and LPIPS of the marker field. Results averaged over 3 runs.

## F BUOYANCY-DRIVEN FLOW WITH OBSTACLES

### F.1 TRAINING

We train all networks with Adam and learning rate  $10^{-4}$  with batch size 16. We begin with training with a sliding window size  $S = 2$ , which we increase every 30 epochs by 2 until we reach  $S = 20$ .

### F.2 ADDITIONAL RESULTS

We give additional results in figure 19. Compared to figure 9 these contain two new variants. We now also consider the *SDE training*, where noise is included in the multi step loss, as well as an additional variant based on the backward only probability flow training, named *Backward only + physics conditioned*. For this method, we extend the input dimension of the score function to accept concatenated inputs of the form  $s_\theta([\mathbf{x}, \mathcal{P}(\mathbf{x})], t)$ , which allows the network to access additional information regarding the physics implemented in  $\mathcal{P}$ . Overall, methods that train based on the probability flow as proposed in section 3 (probability flow training and the backward only probability flow; no noise is included for multiple steps in the sliding window formulation) attain similar results as the SDE training (with noise included). However, in our evaluation they obtain a significantly lower LPIPS distance than the SDE training for the reverse-time ODE inference, which could indicate some advantages of this approach. Separating the physics and score update performs best here, as this method is the least susceptible to bigger timesteps  $\Delta t$  and inaccurate physics solvers  $\mathcal{P}$ .

Moreover, we provide more detailed visualizations for the buoyancy-driven flow case and the *separating physics and score* variant in figure 21 and figure 22. These again highlight the difficulties of the physics simulator to recover the initial states by itself. The SMDP variants significantly improve upon this behavior.

In figure 20 we also show an example of the posterior sampling for this case. It becomes apparent that the inferred small-scale structures of the different samples change. However, in contrast to cases like the heat diffusion example, the physics simulation in this scenario leaves only little room for substantial changes of the states.

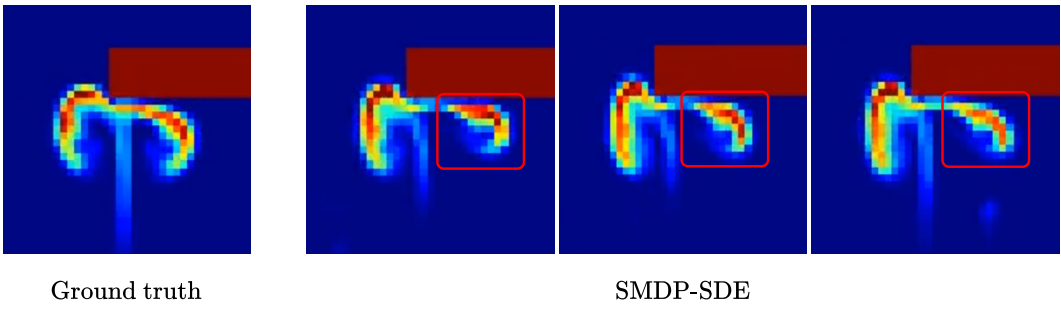
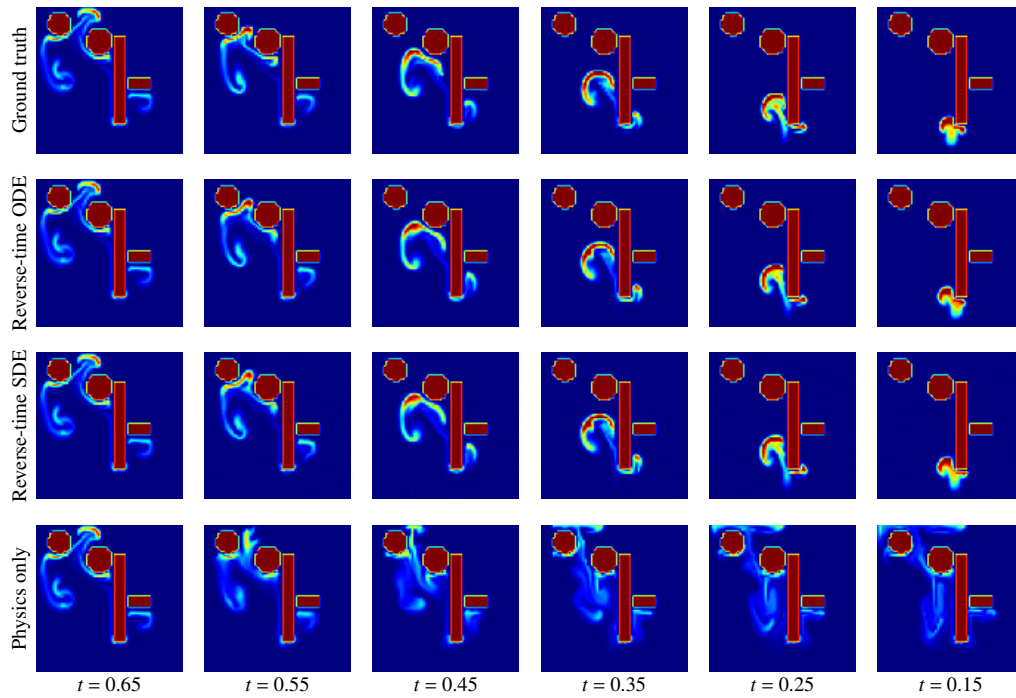
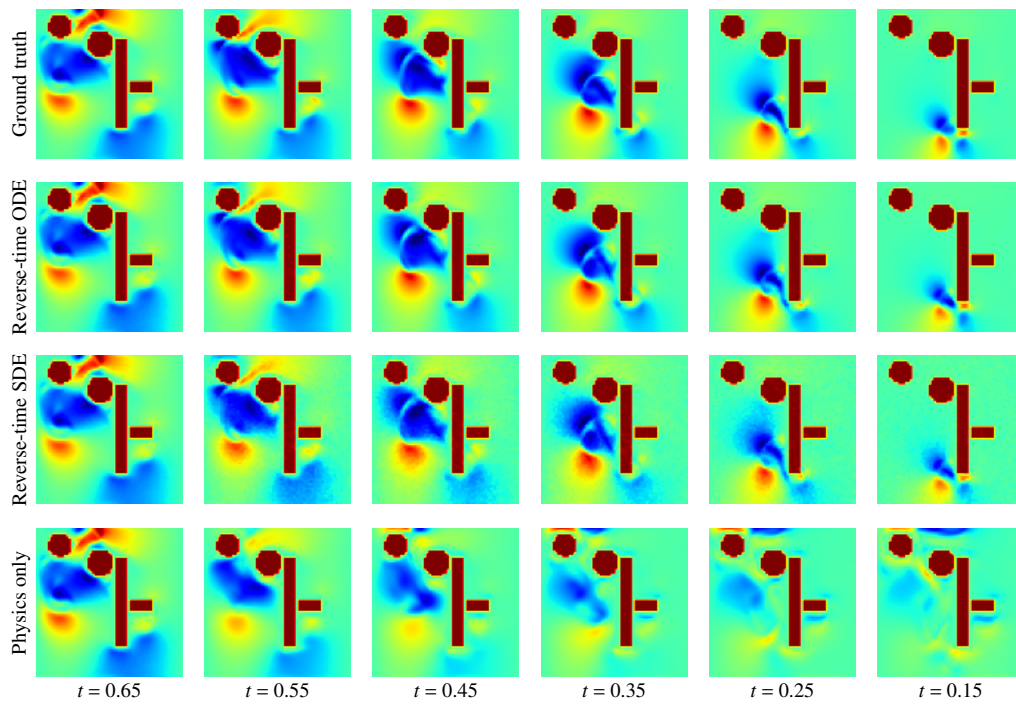


**Figure 20:** Comparison of SMDP-SDE predictions and ground truth for buoyancy-driven flow at  $t = 0.36$ .

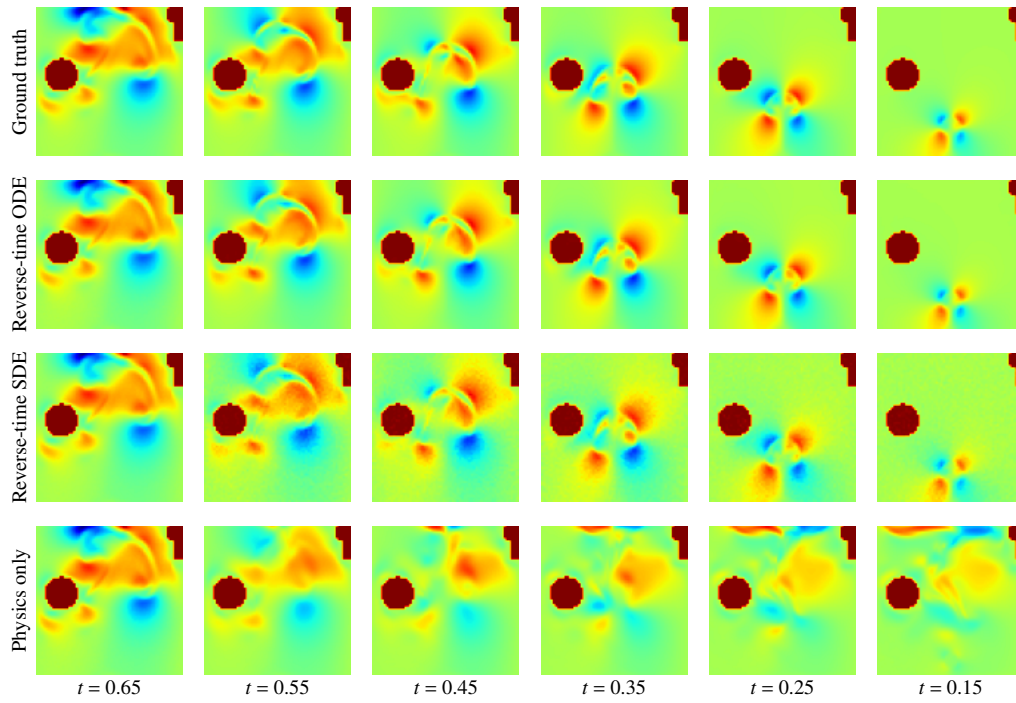


(a) Marker field

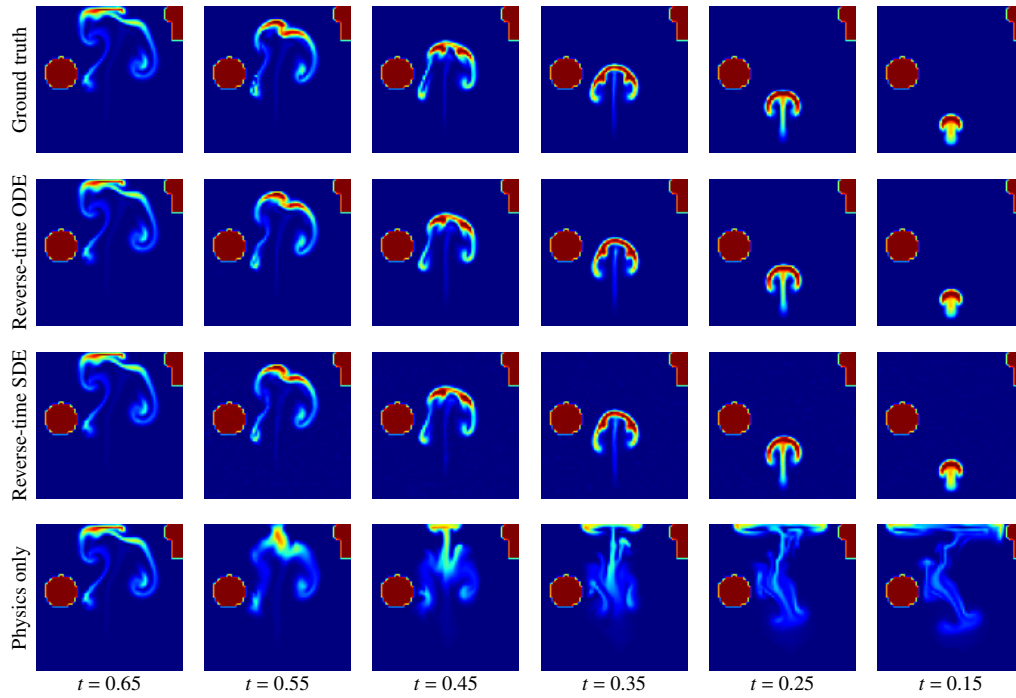


(b) Velocity field ( $x$ -direction)

**Figure 21:** Predictions for buoyancy-driven flow with obstacles (example 1 of 2).



(a) Marker field



(b) Velocity field ( $x$ -direction)

**Figure 22:** Predictions for buoyancy-driven flow with obstacles (example 2 of 2).

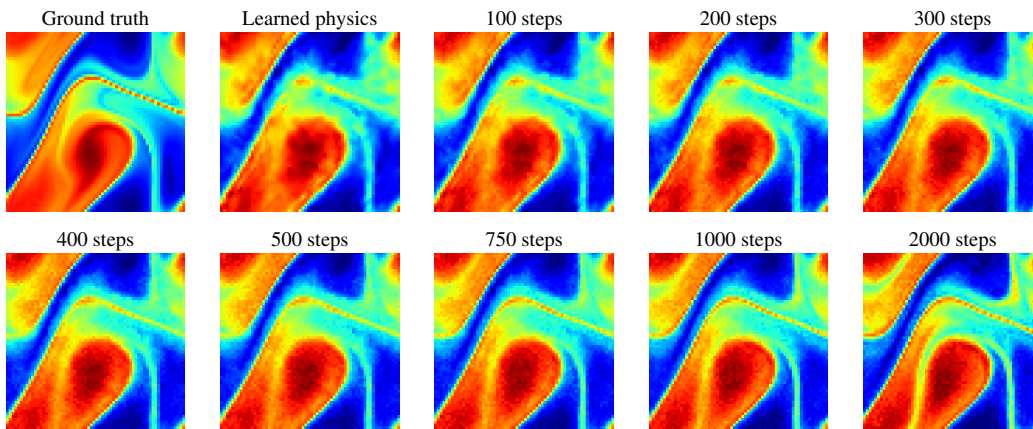


**Figure 23:** Steps of Langevin dynamics for  $\epsilon = 2 \times 10^{-5}$ .

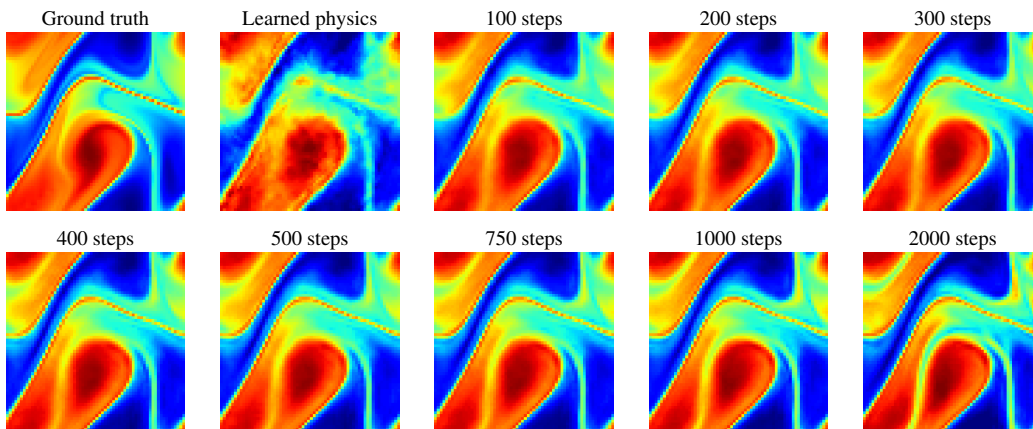


**Figure 24:** Steps with Langevin dynamics for  $\epsilon = 2 \times 10^{-5}$  and an additional step with  $\Delta t s_\theta(\mathbf{x}, t)$  which smoothes the images.

## G ISOTROPIC TURBULENCE

For the learned physics network, we employ a FNO neural network with batch size 20. We train the FNO for 500 epochs using Adam optimizer with learning rate  $10^{-3}$ , which we decrease every 100 epochs by a factor of 0.5. We train  $s_\theta(\mathbf{x}, t)$  with the ResNet architecture for 250 epochs with learning rate  $10^{-4}$ , decreased every 50 epochs by a factor of 0.5 and batch size 6.

### G.1 REFINEMENT WITH LANGEVIN DYNAMICS

We do a fixed point iteration at a single point in time via:

$$\mathbf{x}_t^{i+1} = \mathbf{x}_t^i + \epsilon \cdot \nabla_{\mathbf{x}} \log p_t(\mathbf{x}_t^i) + \sqrt{2\epsilon}z_t, \quad (101)$$

for a number of steps  $T$  and  $\epsilon = 2 \times 10^{-5}$  as a post-processing and refinement strategy, cf. figure 23 and figure 24. This is motivated by established methods in score-based generative modelling (Welling & Teh, 2011; Song & Ermon, 2019). For a prior distribution  $\pi_t$ ,  $\mathbf{x}_t^0 \sim \pi_t$  and by iterating equation (101), the distribution of  $\mathbf{x}_t^T$  equals  $p_t$  for  $\epsilon \rightarrow 0$  and  $T \rightarrow \infty$ . There are some theoretical caveats, i.e. an additional Metropolis-Hastings update needs to be added in equation (101) and there are regularity conditions (Song & Ermon, 2019).

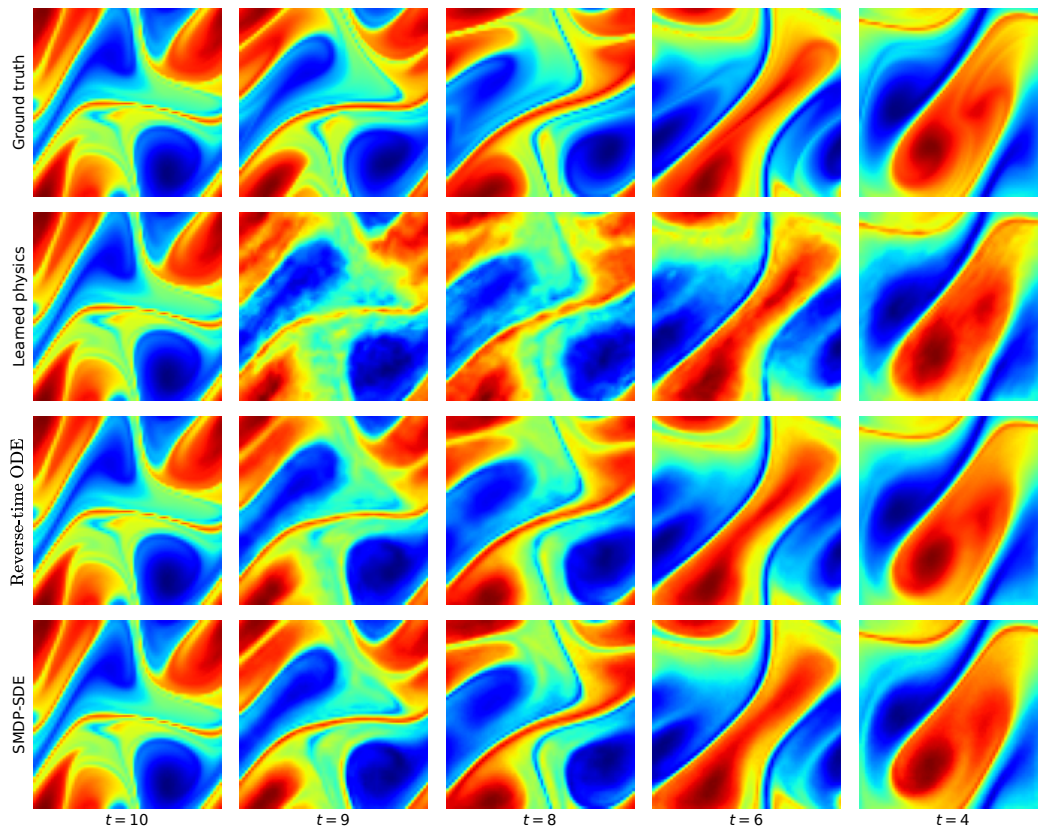


**Figure 25:** Predictions for isotropic turbulence (example 1 of 2).

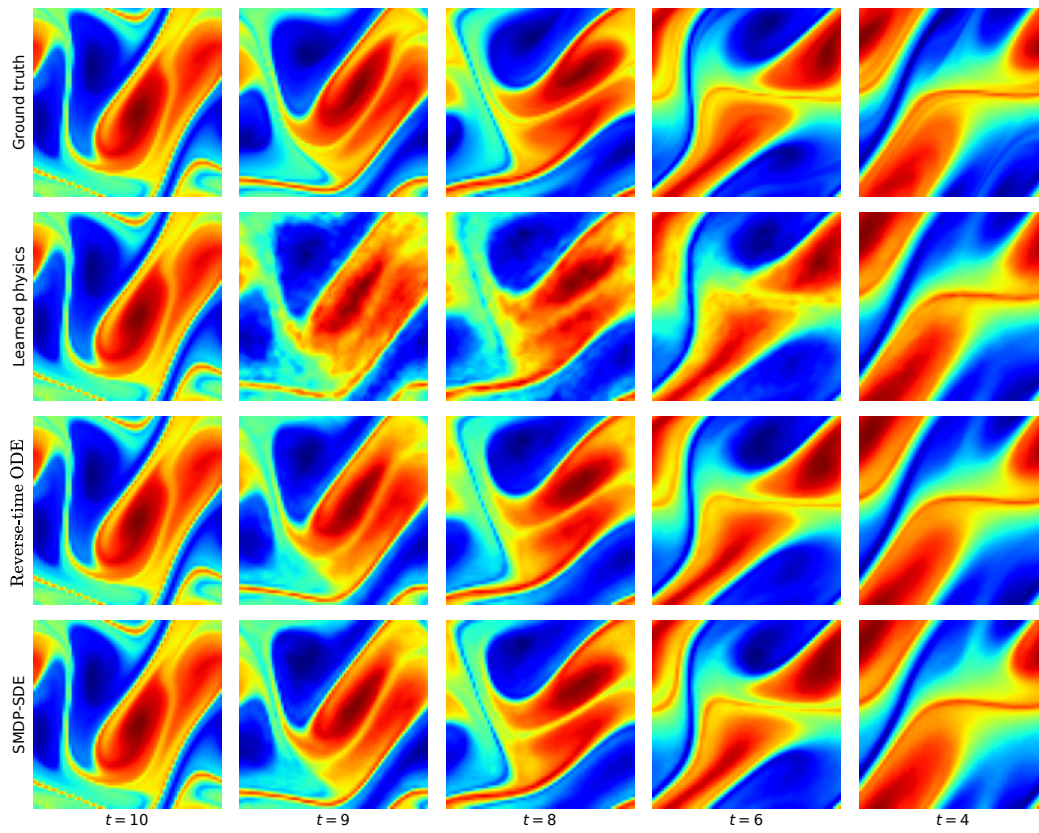


**Figure 26:** Predictions for isotropic turbulence (example 2 of 2).